university of groningen / faculty of science and engineering / biomedical engineering

Design of magnetically actuated surgical devices using magnetic micro-particles embedded in a polymeric matrix

Luis Fernando Peña Samaniego

S-3076296

Surgical Robotics Laboratory (SRL),

Department of Biomedical Engineering, University of Groningen and University Medical Centre Groningen - Department of Biomechanical Engineering, University of Twente

Period: 12/02/2018- 14/08/2018

Thesis for the Master of Science degree in Biomedical Engineering

Supervisors: Prof. dr. Sarthak Misra, Principal Investigator at Surgical Robotics Lab,

Dr. Venkatasubramanian Kalpathy Venkiteswaran, Post-doctoral fellow at SRL

Mentor: prof. dr. ir. G.J. (Bart) Verkerke, Department of Biomedical Engineering

Abstract

Minimally invasive surgery (MIS) has gained popularity in the medical field because the reduction of trauma, pain and recovery time that offers to patients. However, surgical instrumentation used in this approach limits maneuverability and dexterity. Magnetic actuation as a control method provide important advantages such as remote control and fast response, and, since it is safe to use in the human body, it offers a promising alternative for the design of new surgical tools.

In this project, the fabrication of soft magnetic robots and its further actuation under an external magnetic field are investigated with the objective of reproducing controlled motion patterns. Soft robots have flexible and compliant bodies that results in higher degrees of freedom and better adaptability to their surroundings, making them suitable for applications involving soft biological tissue. Magnetic actuation in soft polymers was achieved by mixing ferromagnetic microparticles (PrFeB) with polymer precursors before its curing. The resultant magnetic polymer composite (MPC) was used to fabricate soft robots by a squeegee-coating fabrication technique. Magnetization of the soft robots was done under a uniform 1 T magnetic field. Using different magnetization profiles and the behavior of the external field used for actuation, three different designs, each with a different type of locomotion inspire by nature, were achieved.

The use of soft robots with integrated magnetic actuation in MIS can result in an improvement during task performance, easier control, and reduced possibilities of tissue damage. Future work regarding this project will focus in miniaturization to integrate these notions about locomotion of the samples into the design of surgical tools.

Contents

1 Introduction

Minimally invasive surgery (MIS) was first introduced in 1980s, and marked the beginning of a prominent change in the medical field since then. It has become the latest technique for a number of operations, such as appendectomy, tubal ligation, cholecystectomy, gastric bypass, myomectomy and prostatectomy, where more than 90% of these interventions are now performed through minimally invasive approaches [1][2]. Some of the main advantages that minimally invasive techniques offer to patients include reduction of intervention trauma and lower incidence of post-surgery complications, reduced pain and quicker recovery, shorter hospitalization time, and improved cosmetic results [3]. At the same time, there are also disadvantages from the surgeon's perspective, such as loss of stereo vision and depth perception, diminished hand-eye coordination, prolonged learning curves and training periods, and extended operation times. In addition, the use of instrumentation suitable for MIS is often more difficult to manipulate and usually limits the surgeon's maneuverability and dexterity compared to human hands [4][5]. Hence, using dedicated instruments can provide better functionality and efficiency.

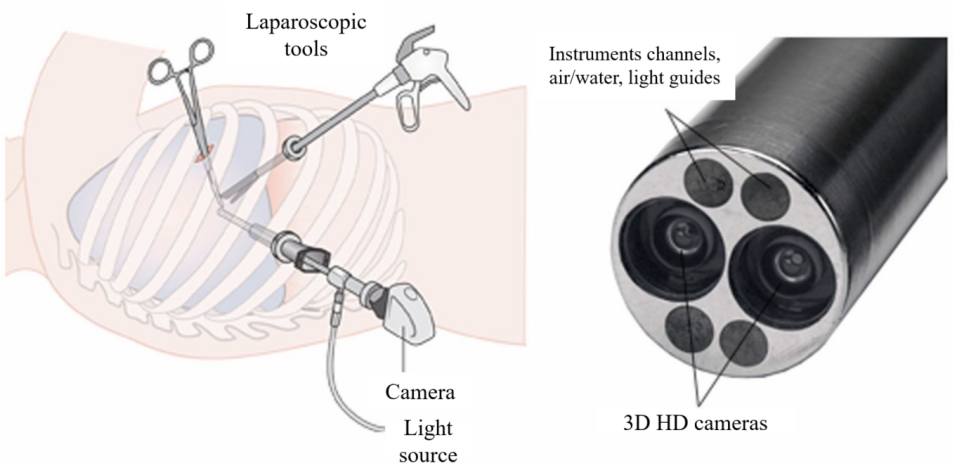

Figure 1: (Left) Representation of how minimally invasive surgery is performed. (Right) Example of an instrument used during MIS: cameras, light source and tools need to be compact in order to be suitable. (Image obtained from [2])

In the last decades, MIS has also benefited by the introduction of robotics systems to assist during surgical interventions, making possible to address some of the aforementioned issues. In robotic-assisted surgery, the use of motors and actuators improve the ability to rotate, move an manipulate the tools [2]. Implementation of tactile sensations and filtering of tremors is also possible. All this contributes to improving task performance, enabling easier control of surgical tools, and integration of multiple sensing sources.

However, designing suitable tools is still a challenge; especially for MIS, where instruments require to be compact and responsive, and have a high level of flexibility and dexterity to maneuver properly in the site of interest [6]. In order to cover these requirements, the use of soft matter has been proposed as an alternative to design surgical tools.

Soft robots have bodies made out of soft and extensible materials with a continuous internal structure which enables them to bend and deform, resulting in high degrees of freedom. They exhibit major adaptation and sensitivity to their surroundings compared to hard-bodied robots, making them able to deal with dynamic environments and simplifying tasks such as grasping and mobility over soft substrates [7][8]. This makes them suitable for applications involving soft biological tissue, where their high compliance help to reduce the damage from contact, adapt to different tissue conditions and safely manipulate delicate objects such as organs and cells.

Actuation for these robots usually involves tendons running along the body of the robot, and pneumatic actuation that inflate channels and cause a desired deflection. Research has focus on the use of other actuation methods to control the soft structures such as shape memory alloys, electric responsive polymers,

and magnetism [8]. Especially magnetic actuation offers a new approach for surgical interventions, some advantages and applications in the medical field are discussed in the next sections.

1.1 Magnetic Actuation

Magnetic actuation represents a promising alternative to other actuation methods since it is a non-contact form of energy transfer, able to provide force and torque over a distance [9]. Given its non-contact nature, it allows for remote control and can be considered as a sterile actuation method [10]. It offers rapid response, and as long as the actuation environment is magnetically transparent, magnetic actuators can operate in many different media, including air, vacuum, conducting and non-conducting liquids, and are unaffected by the ionic concentration of the surrounding medium [11]. Also, it requires no other components, such as power sources, electric wires or other kind of tethers, which leads to favorable possibilities when scaling to micro- and nano-scale [12].

Over the years, the use of magnetic actuation in polymers has been investigated to create actuators and sensors that combine the advantages from magnetic actuation with highly elastic mechanical properties of polymers [12]. Magnetic actuation can be achieved in polymers by incorporating elements with a magnetic dipole moment. These elements are usually made of ferromagnetic materials and can be in the form of micro- and nanoparticles [10][11], thin films [13], spheres or permanent magnets [14][15]. The incorporation of active elements, such as microcoils, is also possible [16]; however, this requires electrical power to be transmitted to the element, limiting the overall contact-free actuation.

In particular, the combination of magnetic particles with a polymer matrix represents a way to create new types of responsive composites. In this magnetic polymer composite (MPC) the magnetic properties mainly depend on the type and morphology of the particles, and the volume fraction of particles used; while the mechanical properties are dictated by the polymer matrix [12][17].

1.2 Applications in Medical Field

The actuation of magnetic elements has contributed to advances in the medical field thanks to the ability to remotely operate such elements in environments with limited accessibility. To date, different applications have been developed using permanent magnets, microcoils and polymer composites to allow magnetic actuation (see Figure 2).

In their work, Yim and Sitti describe the design of an untethered robot consisting of two permanent magnets surrounded by soft elastomer-based structures for controlled drug release inside the stomach [18]. Similarly, Miyashita *et al.* developed an origami robot for patching stomach wounds with a small neodymium magnet attached for controllability [19]. The use of permanent magnets as actuator in a catheter for tip deflection has also been demonstrated in [15].

Microcoils have been used in catheters for tip deflection during magnetic navigation [20][21][22]. Mainly endovascular and cardiac surgical procedures employ magnetic navigation, with results comparable to standard x-ray guidance [23], making this type of navigation an opportunity for interventional MRI and an alternative to ionizing radiation.

The use of MPCs covers a broader field of applications since different structures and different scales can be designed, from micrometric thin membranes to millimeter-scale thick films, allowing applications from drug delivery to soft robots. Pirmoradi *et al.* have developed an implantable MEMS device for controlled drug release based on a thin magnetic membrane [24][25]. Also, soft robots that employ magnetic actuation for motion purposes have been designed. Garstecki *et al.* describe a design able to deform and propel itself in water under the influence of an external rotating magnetic field [26]. Hu *et al.* and Diller *et al.* have both described similar magnetized soft structures able to achieve different types of motions [27][28].

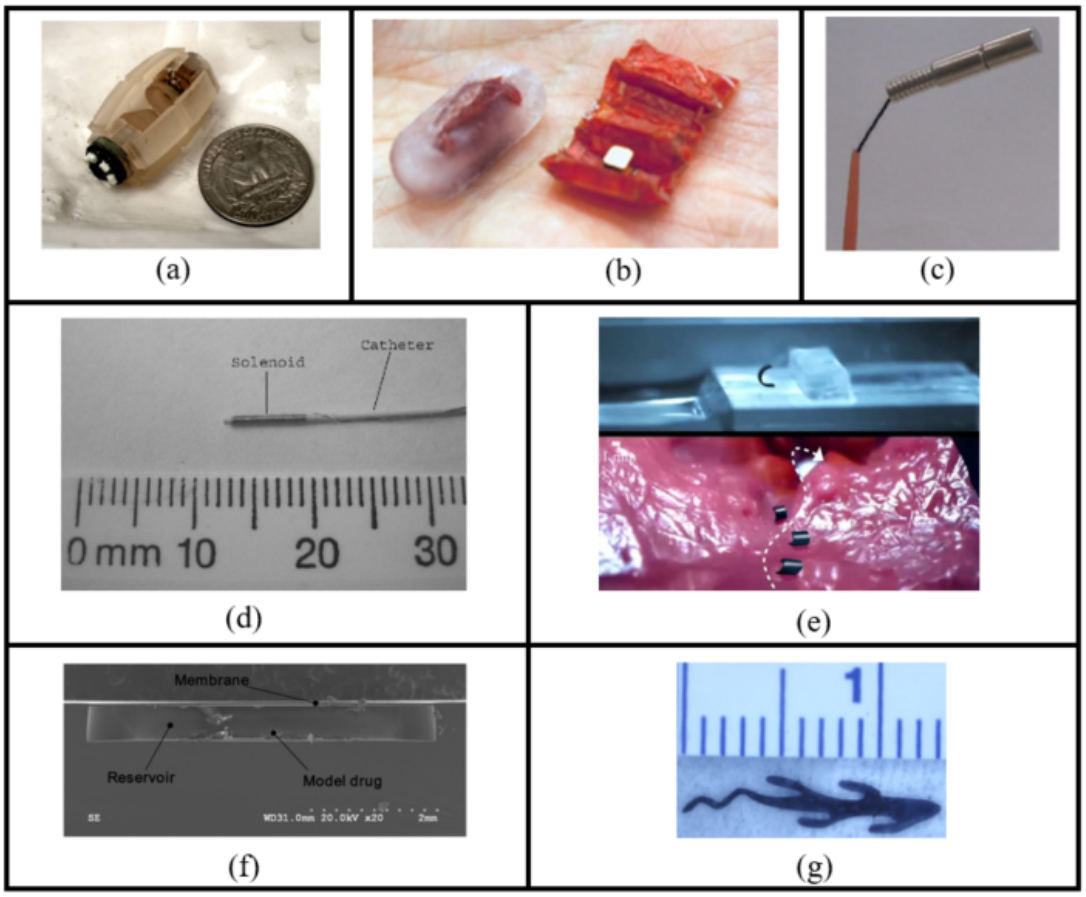

Figure 2: Different medical applications based on magnetic actuation. (a) Capsule with permanent magnets [18]; (b) origami robot with integrated magnet [19]; (c-d) catheters with attached magnets [15] and solenoid at tip [21]; (e-g) Magnetic polymer composite used in for membranes and small robots fabrication.

1.3 Contributions

This study focus on the use of MPCs to design and test soft robots in order to explore different motion capabilities. The motivations for the study are the increase in emerging applications that magnetic composites have in the medical field and the advantages that soft robots can offer to the field of minimally invasive surgery. The actuation of existing soft robots is usually done by tendons and pneumatics, which require a tethered structure. However, with the use of magnetic actuation, this limitation can be overcome. Three different designs are proposed to evaluate different motion patterns based on biological organisms. The designs are fabricated and magnetized in specific profiles to achieve locomotion when expose to an external time-varying magnetic field. This project intends to provide a better understanding on how soft robots can be controlled with magnetic actuation and how further surgical tools can be design applying similar designs.

2 Materials and Methods

All substances are influenced to one degree or another by the presence of a magnetic field. Depending on the response of the atomic magnetic dipoles, materials are classified in diamagnetic, paramagnetic, ferromagnetic, antiferromagnetic and ferrimagnetic [29][30][31].

Ferro- and ferri-magnetic material have inherent permanent magnetic moments due to their atomic dipole distribution. These types of materials are very versatile; some can retain a high magnetic moment after exposition to an external field, and others can be easily magnetized and demagnetized. The reason why ferromagnetic materials possess these properties is the presence of microscopic regions called domains, which align and remain aligned after a magnetic field is applied to the material.

Magnetic polymer composites are usually made using ferromagnetic particles. When it is exposed to an external magnetic field, the particles embedded in polymer interact with the external field. As a result, the polymer can undergo deformation or experience mechanical stress [10][11][12][32][33]. This interaction is described by the following relations:

$$\mathbf{T^m} = \mathbf{m} \times \mathbf{B} \,, \tag{1}$$

$$\mathbf{F^m} = \nabla(\mathbf{m} \cdot \mathbf{B}) \,, \tag{2}$$

where $\mathbf{T^m} \in \mathbb{R}^3$ and $\mathbf{F^m} \in \mathbb{R}^3$ are the induced magnetic torque and force, respectively, $\mathbf{m} \in \mathbb{R}^3$ is the magnetic moment vector, $\mathbf{B}$ is the external magnetic field vector and ∇ is the gradient operator [34].

2.1 Particles

The magnetic element used in this work is an isotropic magnetic powder made from a praseodymium-iron-boron (PrFeB) alloy, with a mean particle size of 5 μm (MQFP-16-7, Magnequench GmbH, Germany) (see Table 1 for detailed composition). Praseodymium (Pr) is a rare-earth element and, since it is a hard magnetic material, possesses a high magnetic remanence; meaning that low external magnetic fields are expected to have some influence over the material. The principal magnetic properties of the selected product are shown in Table 2.

Table 1: Product MQFP-16-7-11277-089 content

Substance	Concentration, Weight %
Neodymium	0.4
Praseodymium	20.6
Boron	1.0
Cobalt	4.1
Niobium	0.4
Iron	73.5

Table 2: Principal magnetic properties from product MQFP-16-7-11277, Magnequench

Magnetic characteristic	Value	Unit (SI)
Residual Induction, B_r	960 – 1000	mT
Energy Product, $(BH)_{max}$	124 – 140	kJ/m3
Intrinsic Coercivity, H_{ci}	520 – 600	kA/m
Coercive Force, H_c	460	kA/m
Magnetization Field to >95% saturation (min.) H_s	≥1600	kA/m
Curie Temperature	345	°C
Maximum operating temperature	80 – 120	°C
Maximum process temperature	200	°C

2.2 Polymer

A variety of materials can be used for the polymer matrix. Commonly used materials include hydrogels, silicones, polyurethanes and rubbers [12]. In order to qualitatively compare how the mechanical properties influence the soft magnetic structures, three different materials are chosen. These materials are (a) silicone rubber (Ecoflex™00-10, Smooth-On, Inc., USA), (b) urethane rubber (PMC®-770, Smooth-On, Inc., USA) and (c) silicone elastomer (PDMS) (Sylgard® 184, Dowsil™, USA). Relevant mechanical properties of the materials are listed in Table 3.

Table 3: Properties of interest from the materials used. *Young's Modulus value for PDMS was taken from results reported in Johnston *et al.* [35].

Property	Ecoflex™00-10	PMC®-770	PDMS
Specific gravity	1.04	1.04	1.04
100% Modulus (psi)	8	250	191 – 297*
Tensile strength (psi)	120	750	1025
Mixed viscosity (cP)	14 000	3 000	3 500
Elongation at break (%)	800	750	120
Mixing ratios (weight)	1A:1B	2A:1B	10A:1B
Curing time at 25°C (h)	4	16	48

2.3 Fabrication

Preparation. The three polymeric materials consist originally of two liquid precursors that need to be mixed and cured to obtain the final polymer (mixing ratios for each material are given in Table 3). Additionally, the matrix and the particles are mixed at 1:1 and 2:1 weight ratios, for testing purposes. Manual stirring is performed until a homogeneous paste is formed.

Immediately after the mixing, the magnetic composite is degassed in a vacuum chamber to eliminate air bubbles. Once this process is completed, the composite is poured into the corresponding molds trying to keep a slow constant pouring rate to prevent the formation of new air bubbles.

Squeegee-coating. The fabrication method selected to create the polymeric structures is called squeegee-coating. This method is described in the work by Wang *et al.* [9] and Pallapa *et al.* [36]. Some advantages of squeegee-coating include less dependence between the viscosity of the paste and the minimum feature size that can be achieved, and that there is no need for specific devices such as a spin caster or inkjet printer in order to complete the process. Also, since the molds can be prepared using common techniques like lithography, laser ablation, 3D printing, etc., features with different depths can be achieved in one single mold. (See Appendix C for further information on fabrication techniques)

When the composite is poured into previously prepared 3D printed and acrylic molds, it slowly flows through the cavities of the mold. After the mold is completely filled with composite, the excess material is removed by passing a squeegee blade across the surface of the mold. After the necessary curing time, the MPC can be easily peeled off from the mold.

2.4 Magnetic Results

Measuring the magnetic properties. A Vibrating-Sample Magnetometer (VSM, Quantum Design Inc) is used to evaluate the magnetic properties. The device measures the magnetic moment of a sample based on the flux change in a coil when the magnetized specimen is vibrated near it. For this purpose, samples of 4x4 mm and a thickness of 0.5 and 1 mm are prepared. The samples are fixed onto a quartz probe and inserted into the device. The data acquisition is done with a maximum and minimum external magnetic field of +3 and -3 T, respectively, in order to surpass saturation (95% saturation at 2 T according to supplier). The data acquisition rate is increased between +0.5 and -0.5 T in order to obtain more detailed information of

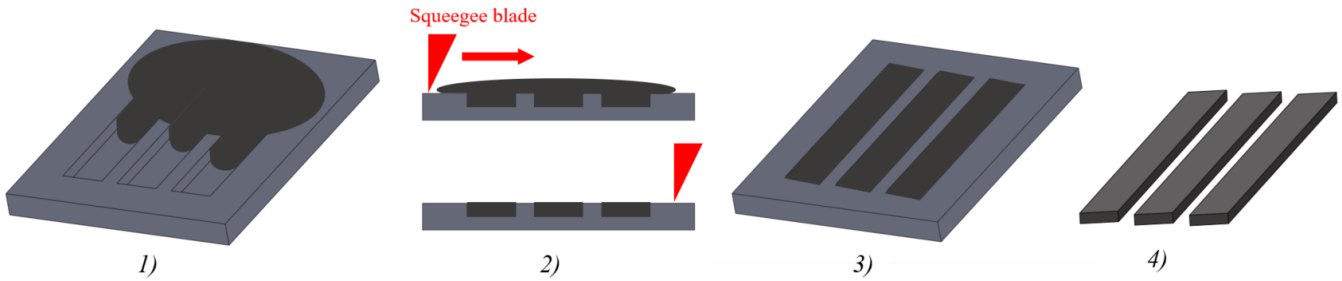

Figure 3: Squeegee-coating process. 1) Material is poured so it can flow through the mold. 2) Excess of material is remove passing a squeegee across the surface. 3) MPC cures on the mold. 4) The resulting structures can easily peeled-off from the mold.

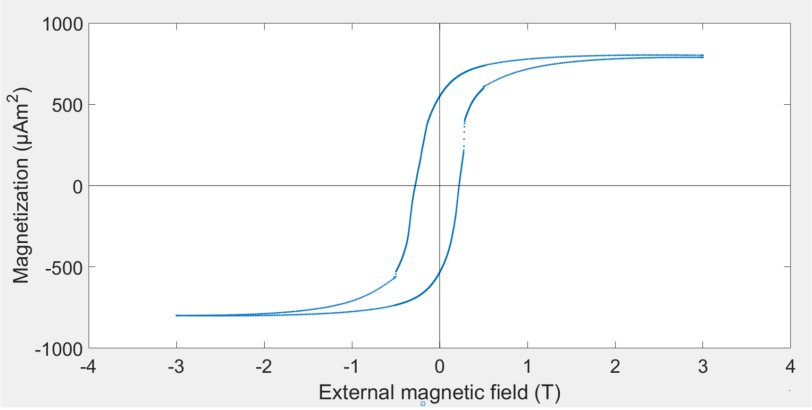

Figure 4: Corrected M-H curve obtained from a 4x4x0.5 mm sample. The polymer used was Ecoflex 00-10 mixed in a 1:1 weight ratio with magnetic particles.

the values where the plot cross the abscissa and ordinate axis (See Appendix A for more detailed information on the obtained plot). After proper corrections, an M-H curve is obtained with clear hysteresis behavior, characteristic of ferromagnetic materials (Figure 4). (See Appendix D for the detailed data analysis process)

Magnetization. The magnetization of the MPC is performed under a uniform magnetic field generated by high power Helmholtz coils (B-E25, Bruker) (Figure 5). The maximum field generated by this system is 1 T, meaning that even when magnetization is achieved, the sample with PrFeB particles does not reach saturation state.

The magnetization of the sample occurs instantaneously during the exposition to the external field; the duration of the process is given by the time that the system takes to go from zero field to the maximum field, and return back to zero field. In order to keep the sample in the desired position during this lapse, acrylic holders are designed with the desired magnetization profile.

Preliminary tests. After the magnetization process, the samples are subjected to qualitative tests with different supports and holders that use one or two permanent magnets as a source of external magnetic field. Figure 37 and Figure 38 shows some of these tests with different profiles and different materials, respectively. The objective of these preliminary tests is to observe and compare the response of different magnetization profiles in samples made from the different polymeric matrices and with different particle ratio concentration.

From the tests, and as expected, it can be observed that Ecoflex samples exhibit higher deformations, being able to bend and adopt the magnetization profile. On the other hand, the samples made of PMC and PDMS have similar results, they are able to bend in the direction of the magnetic field, however, their higher Young's Modulus does not allow pronounced deformation. For this reason, the design of future magnetization profiles and its interaction with an external magnetic field will take the deformation that can be achieved with Ecoflex.

Further experiments are performed in a system called BigMag, which is briefly introduced in the next section.

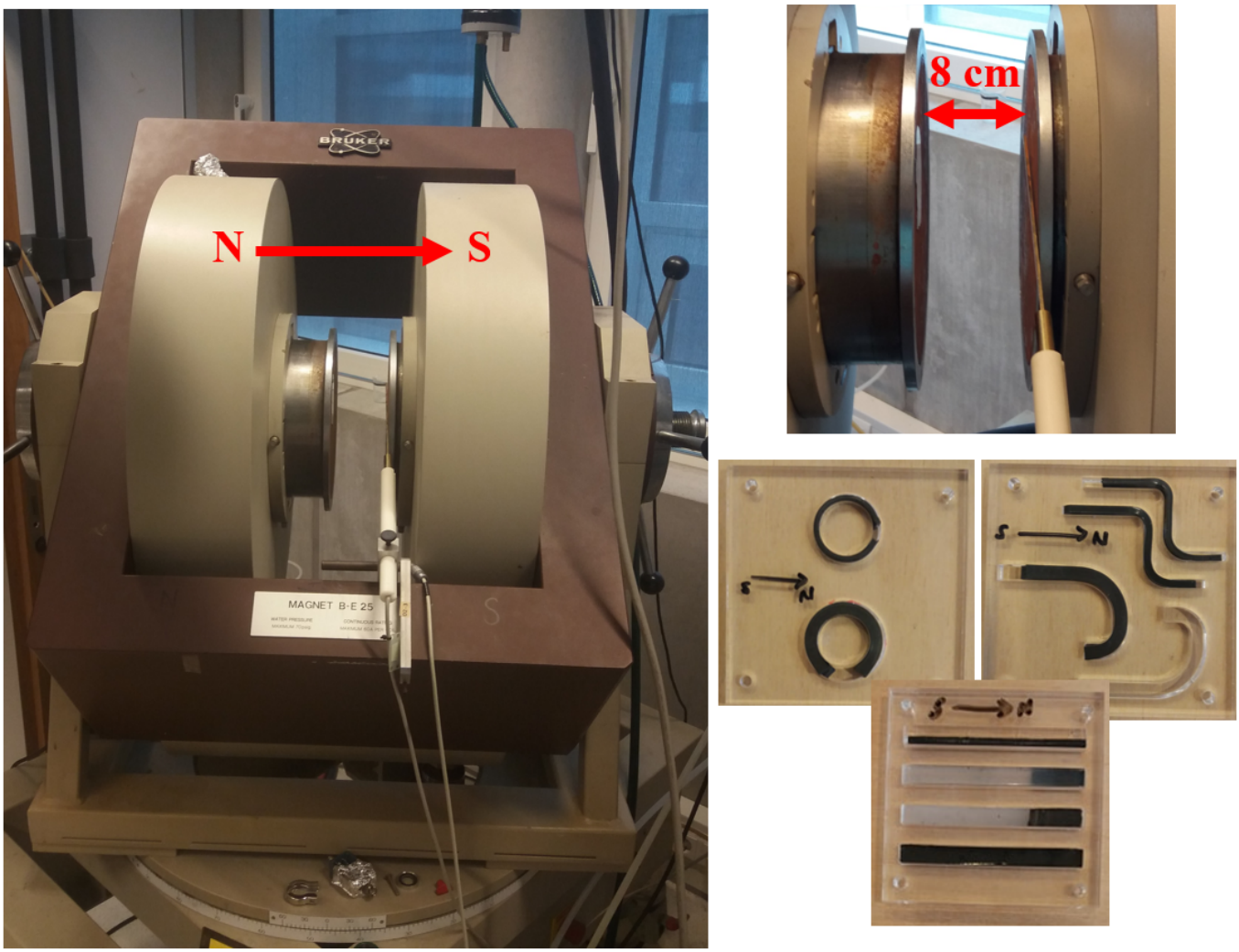

Figure 5: (Left) Helmholtz coils system used for the magnetization process; red arrow indicates the direction of the generated magnetic field. (Right top) Functional workspace. (Right bottom) Samples on acrylic holder. The black arrows on the holder indicates the direction of the magnetization.

BigMag. In this work, the actuation is achieved using an array of six electromagnetic coils called BigMag [37]. The coils can rotate around a spherical workspace with a diameter of approximately 10 cm. The system is capable of producing magnetic fields of specified magnitude and direction at any point within the workspace.

The system is divided into two symmetrical frames located above and below the horizontal central plane of the workspace with three coils on each frame (Figure 8). This arrangement allows them to rotate independently around the workspace in order to change the direction of the field. The system also has two cameras for visualization of the workspace — one for the top view and another for the side view.

The interface with BigMag is done via C++, where parameters like intensity, initial direction and desired rotation of the magnetic field can be defined. Desired changes in the previous mentioned parameters can also be programmed. In most of the experiments conducted during this project, the magnetic field was generated in the xz-plane of the workspace, and programmed to rotate around the y-axis.

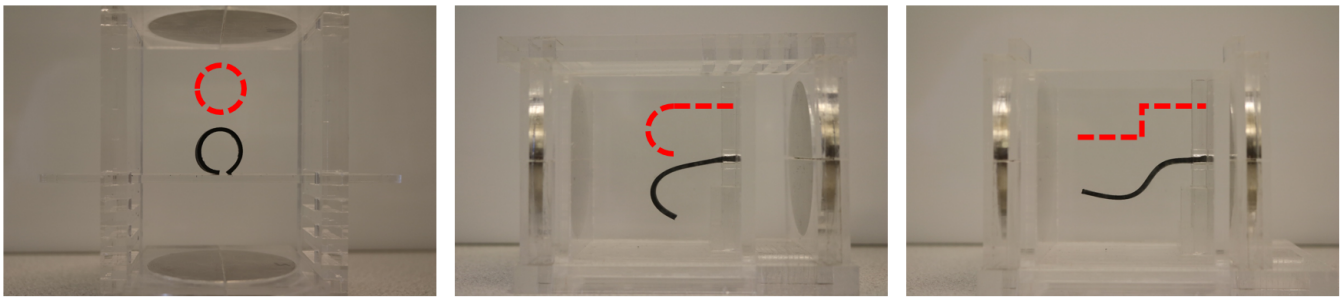

Figure 6: Ecoflex samples at 1:1 weight ratio with magnetic particles. Each sample deforms according to the magnetization profile (shown in red dashed curves) when exposed to an external field.

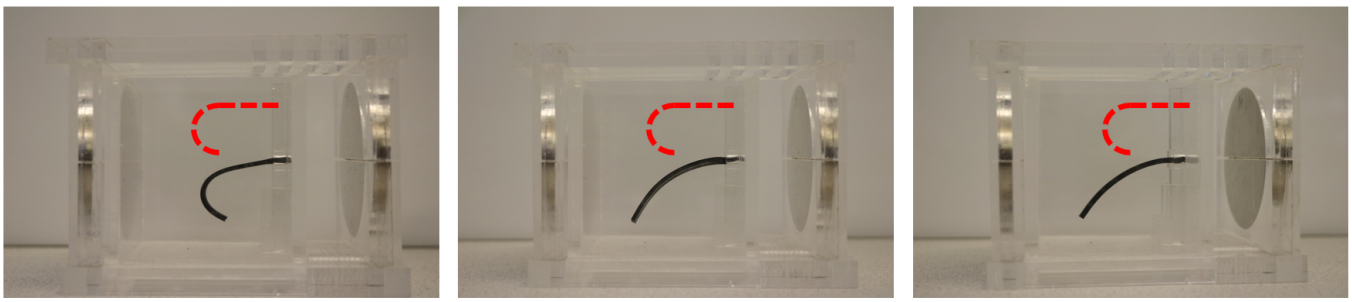

Figure 7: Same magnetization profile (indicated in dash lines) using different polymers: Ecoflex (left), PMC (middle), and PDMS (right). Ecoflex and PMC samples are made at 1:1 weight ratio; PDMS sample is made at 2:1 weight ratio. Ecoflex sample is the only one to deform accordingly to the magnetization profile thanks to its high compliance.

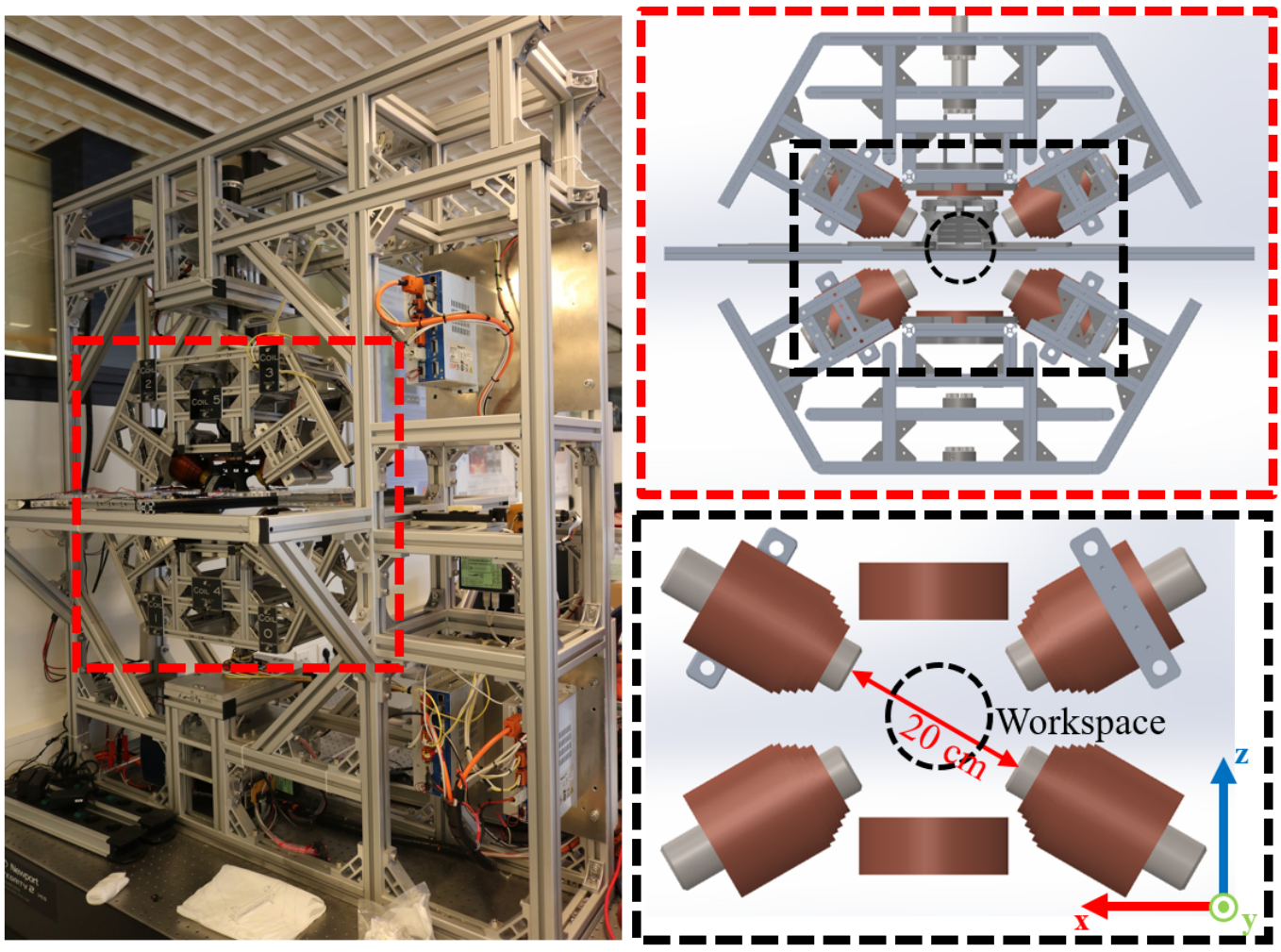

Figure 8: (Left) BigMag system. (Right top) Top and bottom frames of the system. (Right bottom) Workspace model with the corresponding axes and the different BigMag elements indicated in dash lines.

3 Magnetization profiles for motion

Chapter 2 explored the magnetization process of the samples, the effect of mechanical properties on the magnetic response and the experimental setup for demonstration of motion. This Chapter focuses on the design of different magnetization profiles for the selected materials to achieve defined and controlled motion patterns with time-varying external magnetic fields.

3.1 Motion pattern selection

Nature has always been a source of inspiration. Softness and body compliance are features often exploited by biological system in a simple and efficient way [8]. Worms are good examples of remarkable functional locomotion system [38][39], and one of the most studied motions is the one described by the small inchworm. This motion has inspired the development of both soft and hard-bodied robots. In their work, Kotay and Rus [40] describe the design and functioning of a hard-linked inchworm robot. At the same time, other studies has applied similar motion principles to develop soft structures; Seok *et al.* present a soft robot with peristaltic movement made of a tubular mesh and actuated using a coil wrapped around it [41]; similarly, Lin *et al.* describe a caterpillar-inspired locomotion robot [42]. This motion has been also introduced in endoscopic medical devices laparoscopy [7] and colonoscopy [43][44].

Another well studied locomotion pattern is the one described by most of the insects, the tripod gait. Although it has mainly been used in traditional robots [45][46][47], it might give an insight for future multi-legged systems. To date, soft robot with multiple legs are usually composed of only four. In their work, Shepaerd *et al.* describe one of this quadrupedal robots able to achieve different gait patterns using pneumatic actuation [48]. Similarly, Drotman *et al.* present also a pneumatically actuated robot capable of navigating different terrains [49].

In nature is also possible to find more multi-legged animals with unique motion patterns, millipedes and starfish for example, have hundreds of feet, and they are able to coordinate them all to achieve motion. Similar systems were not found in literature, however, cilia-like structures actuated magnetically described in [50], [51] and [52] shows that coordination between adjacent structures can be possible to achieve.

Based on the above, three different designs are selected and named 1) inchworm, 2) spider, and 3) millipede, in reference to the motion patter they are intended to mimic. The fabrication of samples for each design is described next and experimental results are discussed in the next section.

3.1.1 Inchworm sample - Continuous motion

Two different sets of inchworm samples are made, one set made out of Ecoflex, and the second one made of PMC. In both sets, the mixing with the microparticles was done at 1:1 weight ratio. The magnetization profile can be observed in Figure 9. After the magnetization, the sample can be divided in two symmetrical parts, each with two sections: *body* and *leg*. The magnetic moments of these sections are orthogonal to each other; this allows, for example, the *body* sections to align vertically while the *legs* remain horizontal in the presence of a uniform vertical field. During the movement, the *legs* act as an anchoring system, while the *body* generates the necessary propulsion.

When a uniform external field is first introduced at an angle $\theta>0°$ with respect to the horizontal, each section experiences a magnetic torque that tries to align it with the external field. This torque anchors one of the *legs* and partially lifts the other one (the leg that anchors first will be refer as front leg, since the movement is given in that direction; the other will be called rear leg). At the same time, the *body* sections lift until one is aligned with the field. When the field rotates, the *body* continually aligns with the new direction, making the sample move in the direction of the front *leg*. Once the field reaches an angle $\theta>90°$, the front *leg* lifts and the rear *leg* anchors, and the second section of the body starts aligning with the field, allowing the movement to continue. The described motion is shown in Figure 11 using one of the Ecoflex samples and a hand-held permanent magnet (S-60-05-N magnet, Supermagnete, Germany).

The PMC samples are not able to deform in the predetermined profile because of its higher stiffness. Two new designs are made with flexure joints in order to facilitate the deformation (Figure 10). The first of these designs is originally horizontal with parabolic indents on both surfaces where the joint sections are. In the second design, the *body* sections are made in an arched shape, with circular indents at the joints. The magnetization profile from these two new designs of PMC is identical to the previous one.

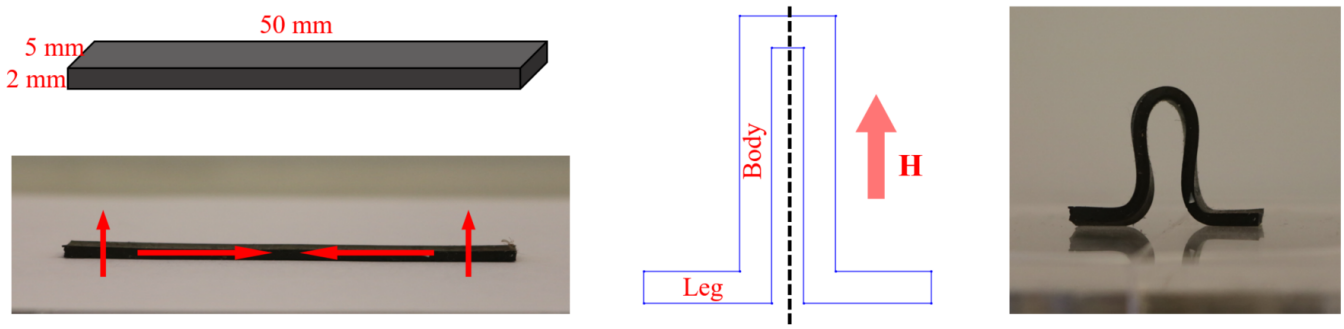

Figure 9: Inchworm sample with the magnetic moment of each section indicated with red arrows (bottom left) and the corresponding magnetization profile (middle). When the sample its exposed to an external field, it deforms according to the magnetization profile (right).

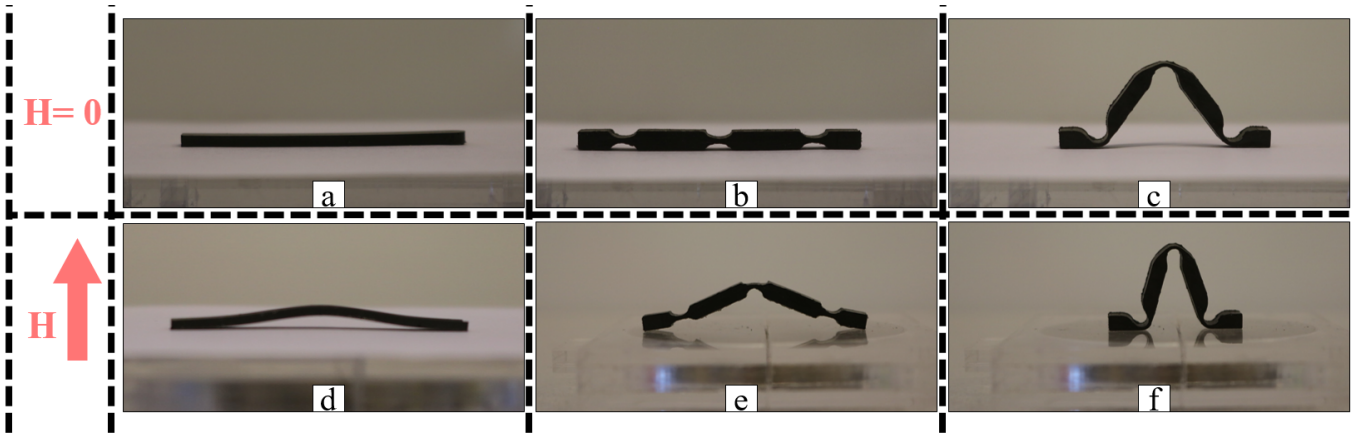

Figure 10: Different PMC designs: (a) original design, (b-c) designs incorporating flexural joints. Images a-c shows their original shape. Images d-f shows the deformation achieved in the presence of a vertical magnetic field.

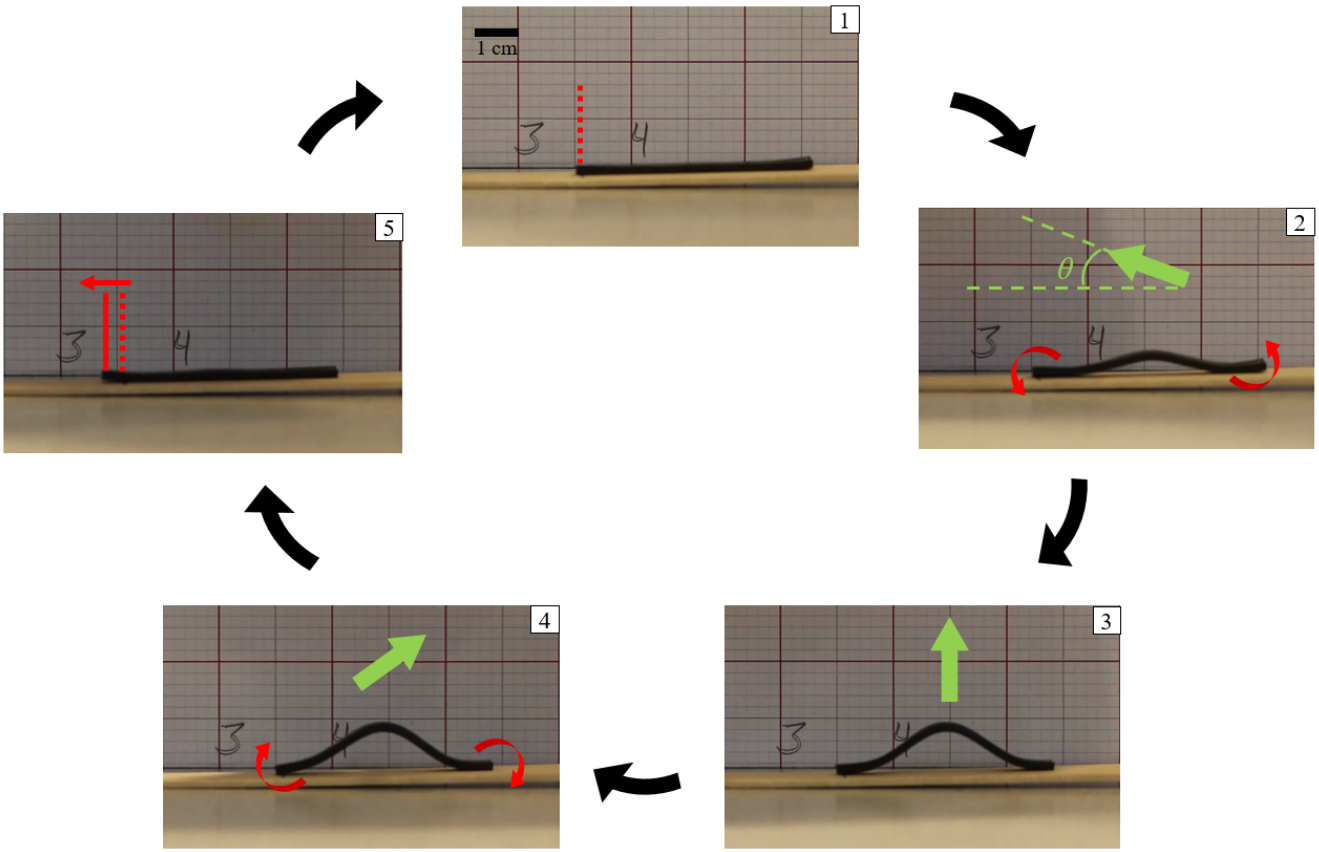

Figure 11: Phases in the crawling motion achieved with a permanent magnet. Depending on the initial direction of the magnetic field, the motion can be performed to the left or to the right (pictures illustrate motion to the left). Direction of the external magnetic field is indicated with green arrows. 1) Original position of the sample. 2) Initial body lift when an external field is introduced, allowed by the anchoring of the front leg and the lifting of the rear leg. 3) Magnetization profile achieved when the field is completely vertical. 4) Change in function between front and rear leg once the field has rotate θ>90°. This allows the sample to slide forward to continue the motion. 5) The sample completes the motion by sliding forward when the field is retired and it is ready to start a new cycle.

3.1.2 Spider - Multi-legged motion

For the multi-legged design, a set of four identical legs are made and magnetized separately, and finally assembled together with a non-magnetic body. Each set of legs is fabricated using either Ecoflex or PMC at 1:1 weight ratio with the microparticles. Samples of two sizes are fabricated: small spiders (around 2 cm), and big spiders (around 6 cm).

For the small spiders, legs are magnetized in a circular profile and in the same direction, meaning that the four legs have identical profiles. Two small spiders are prepared. Spider1 is made with an Ecoflex body and the legs assembled so the profile is projected on the same plane as the body. Spider2 is made with melted hot glue body and the legs assembled so the profile is projected in the transverse plane of the sample (see Figure 12).

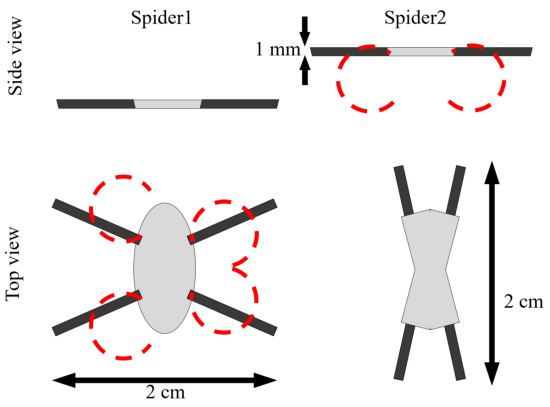

Figure 12: Small spider samples.

For the big samples, each set is magnetized using one of two different profiles: 90° and 180° profile. At the same time, the legs are magnetized in one of two different phases: 0° and 45°. The arrangement of legs to create one sample is as follow. The four legs are magnetized with the same profile (90° or 180°). Two are magnetized in 0° phase, and the other two in 45° phase. Frontal legs use one leg with each phase, in consequence, rear legs do this as well, but in the contralateral side respect to the frontal legs. The intention of this arrangement is to create a synchronous movement between the four legs.

PMC samples require higher magnetic fields than the Ecoflex ones to deform due to its higher stiffness. In this case, no further indentations are made on the PMC legs due to the already low thickness of the samples (around 1 mm). On the other hand, because of the high compliance of Ecoflex, sample thickness is made up to 30 times larger.

3.1.3 Millipede sample - Continuous multi-legged motion

These samples are made using only Ecoflex at 1:1 weight ratio with the microparticles. Unlike the multi-legged samples, the small features in the legs do not allow for separate fabrication, magnetization and assembly. Then, the fabrication process is split into two phases, using one single mold with the desired design.

Initially, the mold is filled with the MPC. After curing, the samples is cut inside the mold, separating the future legs from the rest. Then, Ecoflex is poured into the mold to complete the body of the sample. After curing, the sample is removed normally (see Figure 12). As a result, the sample has legs made of the magnetic composite attached to a non-magnetic body (see Figure 13).

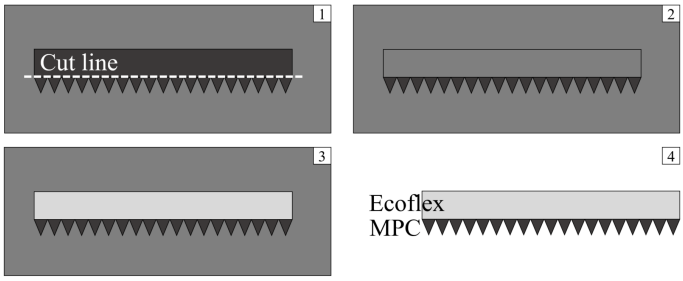

Figure 13: Fabrication of the millipede sample.

In order to create a continuous motion pattern over the multiple legs, magnetization should follow a cyclic profile. Samples are magnetized in circular holders or by wrapping them around cylindrical rods.

3.2 Experiment design and Results

Two magnetic fields are programmed in BigMag in order to test the motion capabilities of the different samples. Both fields are generated in the xz-plane and rotate around the y-axis of the system, and differs

from each other by the range of rotation. The first field is programmed so it does not complete a 360° rotation, while the second has rotations equal or higher to 360°, meaning that the field can start and end in any direction. In both cases, after selecting the desired rotation, cycles are made by repeating this rotation. Table 4 shows the required parameters in BigMag and the defined values for both fields. Figure 4) shows these fields in the workspace of BigMag.

3.2.1 Inchworm sample - Continuous motion

Ecoflex samples. Motion with Ecoflex samples using a permanent magnet was already discussed in the previous section. The magnetic field generated by the magnet and acting on the sample is approximated using COMSOL and Matlab simulations in order to obtain the direction of the field (see Appendix B for more information). As a result, a field starting in an angle of 60° with respect the positive x-axis and ending at 10° with respect the negative x-axis is obtained, meaning that the field rotates 110°. These parameters are used for the first field, in order to generate a crawling motion in the sample. The rest of the parameters are completed using a field magnitude of 12 mT, a cycle duration of 3 seconds, and a time lapse of 3 seconds between cycles. The results of the influence of this first field can be observed in Figure 15, and are comparable to the ones obtained with the permanent magnet.

The second field is programmed starting in direction $-\hat{\imath}$ and able to complete a full rotation with respect to the negative y-axis. In this case, the magnetic moment in each section of the sample continuously aligns with the rotating field, resulting in a complete rotation of the sample as well (see Figure 16). One of the factors that allow this behavior is the high compliance of the sample.

It was noticed that the results depend on the surface on which the motion is tested. The described results were obtained with the sample over a surface made of balsa wood. In contrast, when the tests were repeated on a smooth acrylic surface, the adhesion between the sample and the acrylic was too high, and the movement was not possible.

Table 4: Main parameters of the two magnetic fields. The alternatives options for some of the parameters results in motion in the opposite direction.

Parameter	Field 1		Field 2	
Magnitude (mT)	12		12	
Initial direction	< 0.5, 0, 0.866 >	< -0.5, 0, 0.866 >	< -1, 0, 0 >	< 1, 0, 0 >
Rotation	-110°	+110°	-360°	+360°
Cycle duration (s)	3		2.66	

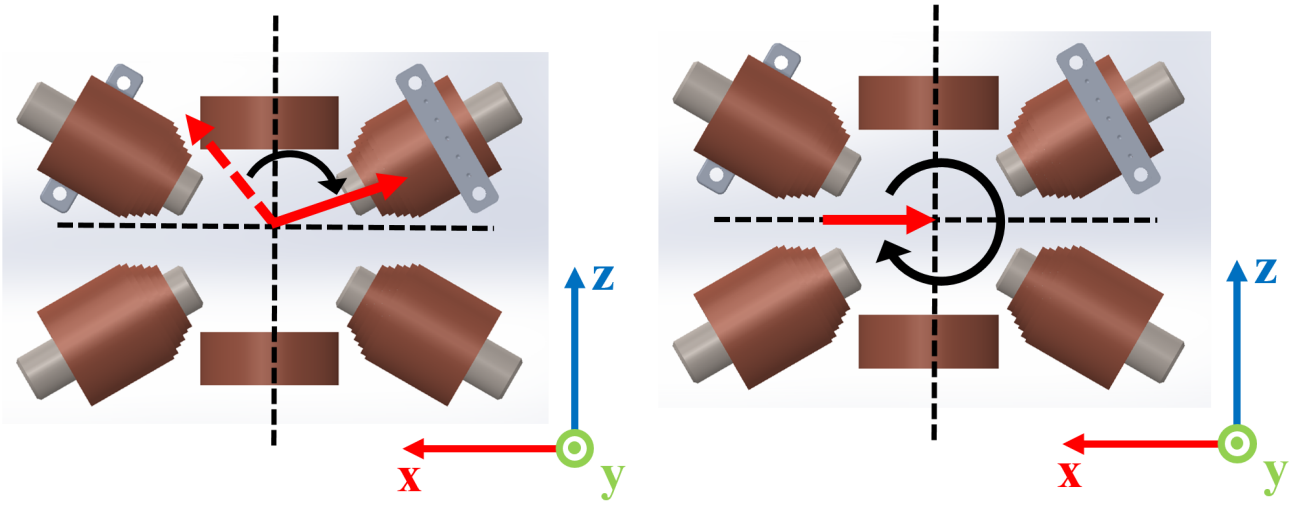

(a) Field 1 (b) Field 2

Figure 14: Magnetic fields programmed in BigMag. The picture shows the initial direction of the field (dash red arrow), the final direction of the field (bold red arrow) and the rotation (black arrow) according to Table 4

PMC samples. PMC designs are only tested using Field 1. The stiffness in these samples does not allow them to roll over themselves. The stiffness also limits the deformation and movement, therefore, higher magnitudes in the external magnetic field are used. However, this increases the possibility of generating enough magnetic force to drag and finally attract the sample to one of the coils.

The original PMC design has the stiffest joints. A maximum external magnetic field of 15 mT is used, however, deformation is almost null and motion is not achieved. Higher values of the external field result in attraction and complete lifting of the sample.

The horizontal design with flexural joints deforms easier than the previous, allowing slightly higher flexion on these points. However, the fields required to make the motion reach values between 25 – 30 mT.

The arch-shaped sample is able to react to fields around 10 mT. However, it does not flex following the motion pattern intended, and even with the flexural joints, the sample is more likely to get lifted than deflected. This situation might be caused by the continuous alignment of the initial *body* section with the external field, even when this rotates more than 90°. This does not occur in the other samples at such low fields because the stiffness at the joints prevents the sample to align with a very steep field, however, in this case, the sample is able to align with a stepper field because of its arched-shape.

3.2.2 Spider - Multi-legged motion

Spider1 is tested using Field 2 continuously (with a magnitude of 15 mT). Since the legs are made out of Ecoflex, they achieve the corresponding magnetization profile and follow the direction of the field during the 360°, allowing them to make contact with the surface during half of the cycle. In this half, the legs are able to lift and push forward the low weight body (see Figure 17 and 18).

Spider2 is tested using only the functional part of Field 2 (the half where the legs make contact with the surface). The body of this sample is heavier because is made of melted hot glue. This affects the magnitude of the field needed so the legs can lift the body, increasing it up to 20 mT.

Since the magnetization profile in the four legs is the same in Spider2, the sample has a certain degree of symmetry with respect to the axial and transverse axis, which allow it to potentially move also in orthogonal direction (left-right) (unlike the inchworm designs, in which only forward and backward motion is possible). Another advantage of this multi-legged design is the reduction of the contact surface between the sample and the substrate during the motion.

3.2.3 Millipede sample - Continuous multi-legged motion

Since these samples have a continuous magnetization profile along its body, Field 2 is used to complete a cycle for actuation. In both samples, single and double wrapped, the constant rotation of the field generates a wave motion, allowing contact between legs and surface only in an specific section of the body en generating a forward motion (see Figure 19). Because of its magnetization profile, the single wrapped sample also experiences a lifting in both ends when the field is vertical; in the double wrapped sample, this is prevented by the neighboring body sections.

Just like the multi-legged design, this design has the advantage of reducing the contact surface between the sample and substrate.

3.3 Discussion

Each sample achieved certain degree of locomotion according to their respective magnetization profile and the direction of the external magnetic field. Also, samples made of Ecoflex showed better results that those made of PMC, mainly due to the difference in the stiffness of the material.

The inchworm samples made of Ecoflex showed a good performance mimicking the intended motion and were also able to achieve a second way of locomotion (rolling). This could be by the fact that the sample is

magnetically divided in four segments, where the magnetic moment of each segment has an specific direction; this results in the whole segment responding in the same way in the presence of an external field.

The millipede samples, unlike the inchworms, have a periodic magnetization profile along theirs bodies, meaning that each part of the body responds slightly different even to the adjacent parts. Nevertheless, these samples also succeeded with the intended motion pattern. Also, thanks to its geometry, the contact surface between the sample and the substrate is decreased, which can result advantageous when the surface is not flat or uniform.

Unlike the previous two designs where the magnetic material was geometrically continuous along the sample body, the design of the spider samples consists in four independent magnetic legs attached to a body in four opposite sites. This required not only to move one leg in the correct profile, but also coordinate the four legs in order for the sample to move. The desired motion pattern was not achieved; however, it was possible to show a certain degree of coordination between the four legs and to achieve a motion in a different way. Because of its geometry and magnetization profile, the contact surface between the sample and the substrate decreased during the movement. And also, thanks to its geometry, there is certain degree of symmetry in the sample which potentially allows it to move in two directions (forward/backward and left/right). Inchworm and millipede samples cannot achieve this.

In most of the samples, the magnitude of the external magnetic field took a value between 10 – 15 mT, only in those samples with higher stiffness the required field for motion increased up to 30 mT. However, the magnitude of the external field can be decreased if the magnetic moment of the samples is increased, and this can be achieved by magnetizing the samples under higher magnetic fields. The samples used in this project were magnetized under a 1 T field, but according to the supplier, the microparticles used to fabricated the MPC reach 95% saturation with a 2 T magnetization field; this value match with the values obtained from the VSM measurements.

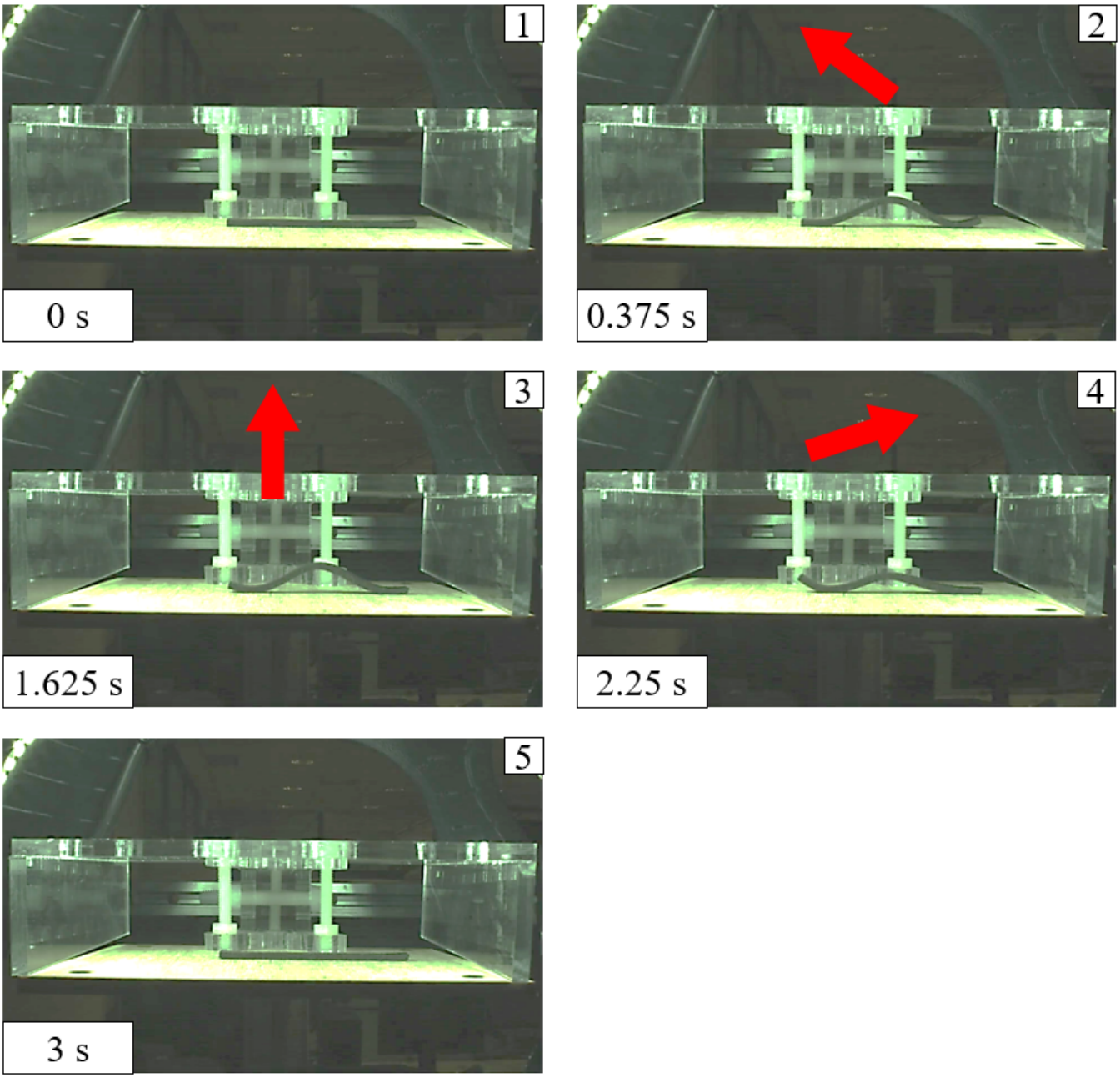

Figure 15: Crawling motion generated in BigMag when applying the parameters of Field 1. The description for each phase can be found in Figure 11. The red arrow indicates the direction of the magnetic field.

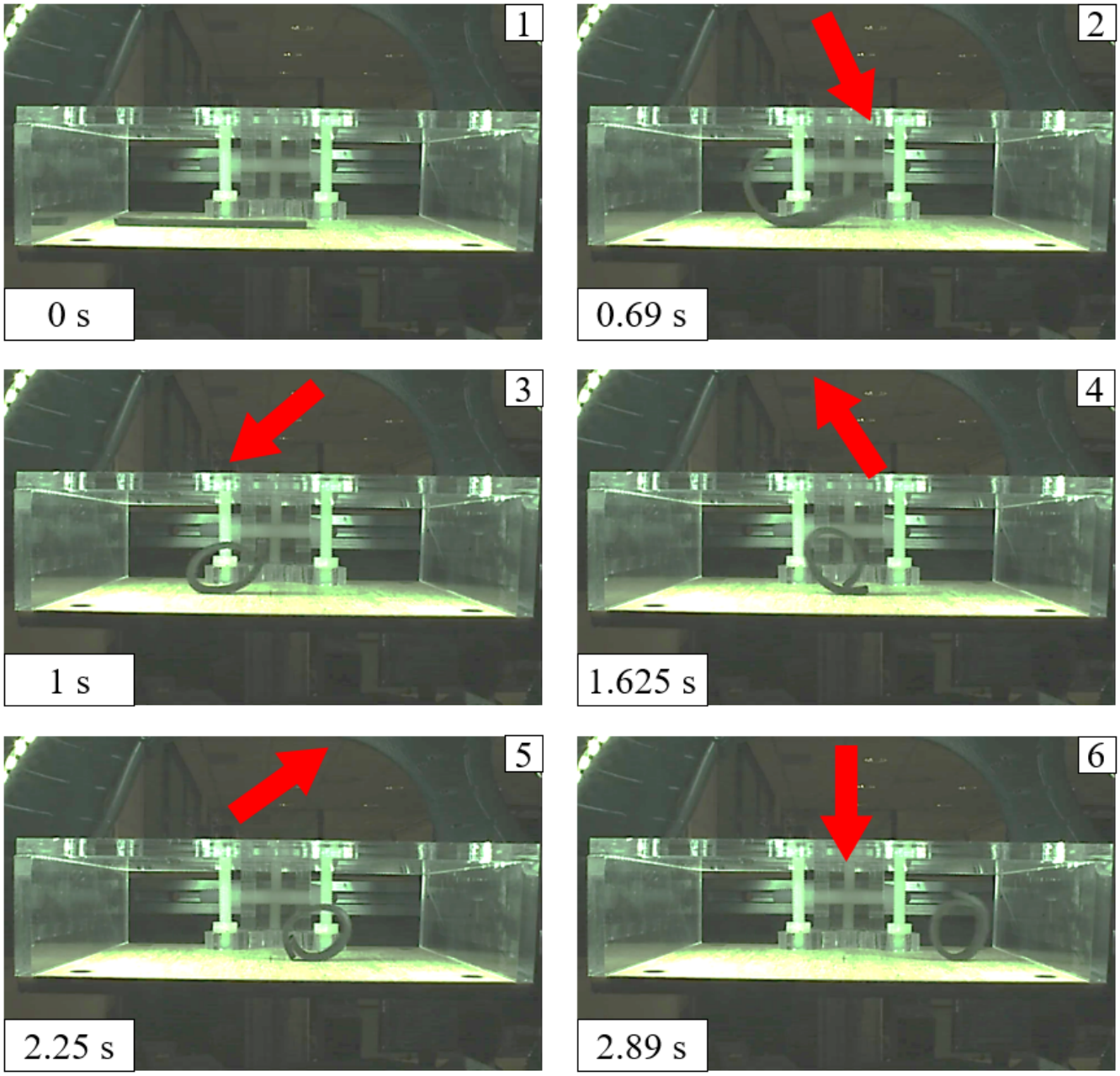

Figure 16: Rotation motion generated when using the parameters of Field 2. When no time lapse between cycles is programmed, the sample is able to continue in a rotation motion. The red arrow indicates the direction of the magnetic field.

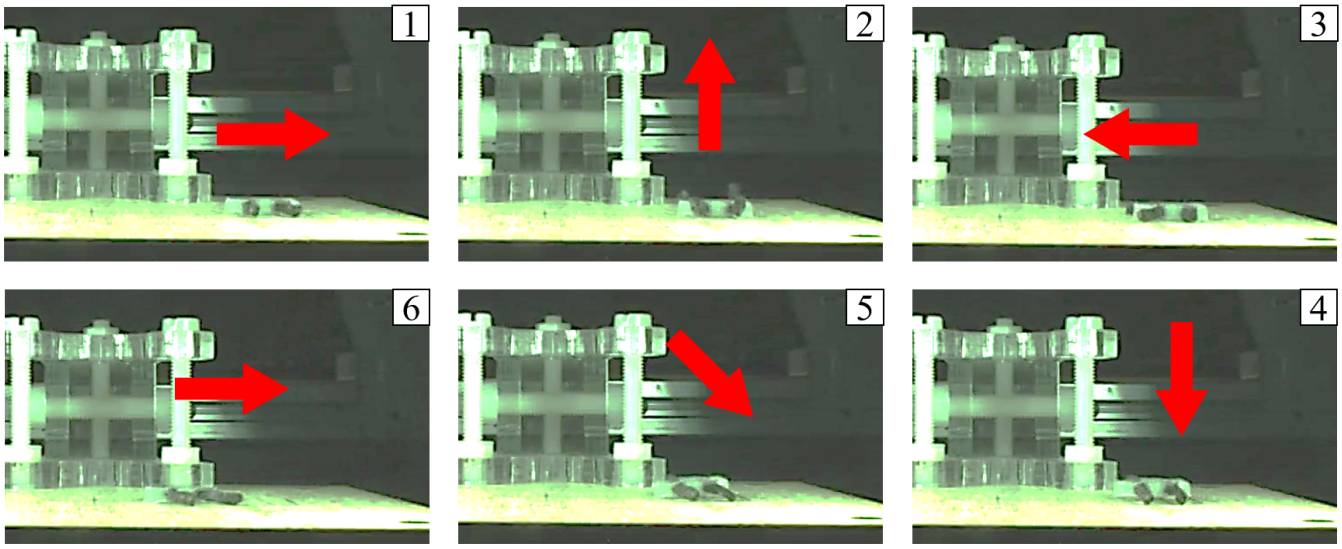

Figure 17: Movement achieved by sample Spider1 in 1 rotation of the external magnetic fileld (red arrows indicate the direction of the field). In frame 4, it can be observed the moment where the body is lifted from the surface, following by the forward motion in frame 5.

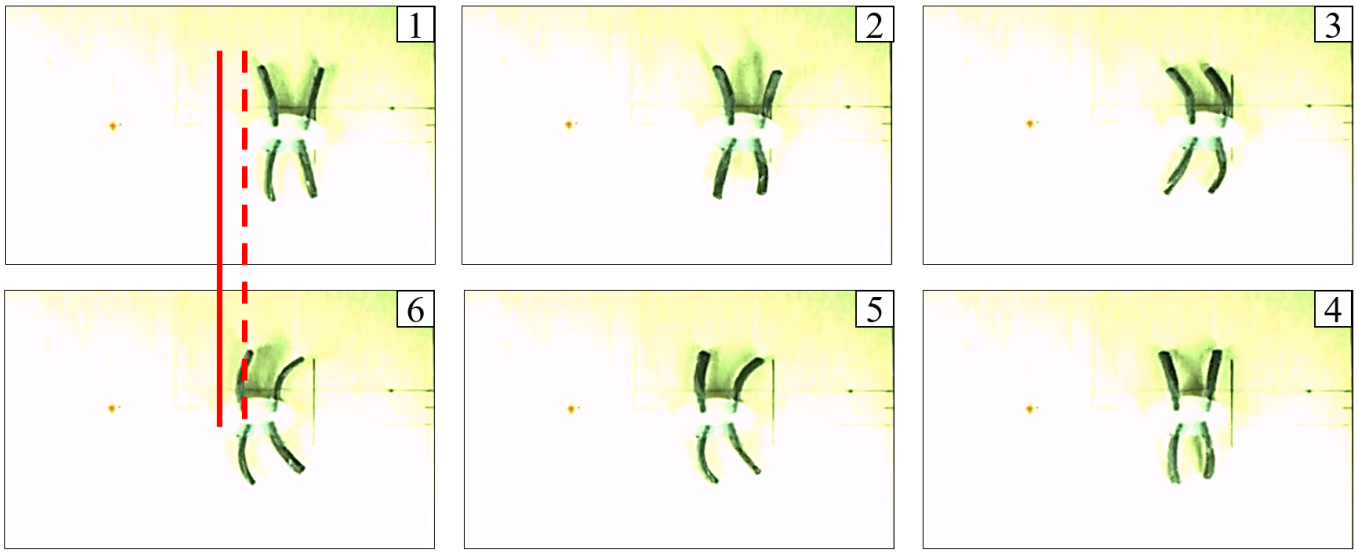

Figure 18: Top view from the same movement frames from Figure 17. Dash and solid line in frame 1 and 6 indicates the initial and final position of the sample, respectively.

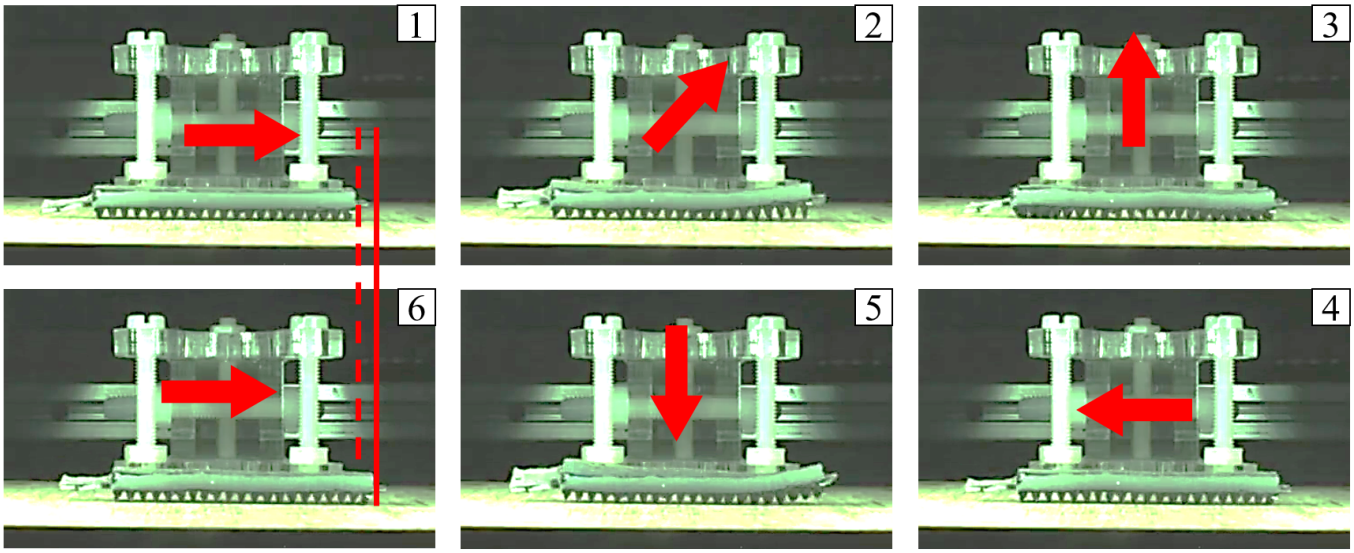

Figure 19: Millipede sample magnetized by wrapping it twice around a wooden rod. The movement is achieved in 1 rotation of the external magnetic fileld (red arrows indicate the direction of the field). Dash and solid line in frame 1 and 6 indicates the initial and final position of the sample, respectively.

4 Conclusions and Future Work

In this work, soft robotic specimens were created to mimic biological motion patterns using magnetic actuation. A magnetic polymer composite (MPC) was created by mixing ferromagnetic particles (PrFeB) with a polymer. Samples made of this MPC were successfully fabricated following a squeegee-coating method. The main advantage of this fabrication approach is its simplicity, since it does not require specific devices to complete the process; and also that samples of different shapes can be easily made by just using different molds. Magnetization of the samples was later possible under a uniform 1 Tesla magnetic field generated by high power Helmholtz coils. From the initial tests, it can be concluded that the response of a sample depends mainly on three aspects: (1) the intensity of the external magnetic field, (2) the volume of magnetic material in the sample, and (3) the mechanical properties of the polymer used.

Based on this, samples were fabricated and magnetized in specific profiles in order to achieve motion. Motion patterns inspired by nature resulted in three different designs named inchworm, spider, and millipede, depending on the sample and the intended locomotion profile. Motion was achieved in the different samples by rotating an external magnetic field in specific directions. Inchworm and millipede samples succeeded in achieving the expecting motion; the magnetic material on these samples is structurally continuous, which helps to keep the entire sample in a certain profile during the deformation. On the other hand, in the spider samples, there is a separation between the four magnetic legs, which imposes an additional challenge on coordinating the deformation in order to perform the movement.

The results of this project show that magnetic actuation is suitable to control untethered millimeter-scale soft robots. It also shows the potential of using soft and deformable structures in order to mimic motion pattern at such scale. Even when the different samples succeeded performing certain motion, some still need optimization in terms of geometry and the correct interaction with the external field. Also, as mentioned with the Ecoflex inchworm samples, the material of the surface plays a role in the motion. Future work should focus in improving these aspects and characterize the relation between the sample and the substrate with the motion, as well as focusing in miniaturization to integrate these notions into the design of surgical tools.

Ethical Impact

The potential outcome of a magnetically actuated surgical tool involves several ethical issues that must be taken into consideration. The introduction of any new technology implies a certain risk to patient safety, which may come both from the procedure and the material itself [53]. Regarding the procedure, surgeons switching to this new technology would be demanded to train and develop a new set of skills in order to successfully perform a surgery. Jeffrey A. Larson [54] points out the current ethical challenges of such training, together with its consequences during a surgery, and provides a set of principles to reduce the risk of harming patients and make the transition ethically acceptable. Such principles involve a proper and continuous mentorship, improved training sessions with real case scenarios and the identification of procedures in which the implementation of this new technology can be more beneficial. As for the material, since the surgical tool is meant to be inside the patient body, alterations to their normal physiology due to material-tissue interactions must be prevented [55]. For such purpose, a biocompatible and bioinert non-toxic polymer coating for the material, which must provide optimal surface properties for the reduction of physiological responses, should be further studied to ensure patient safety.

The real cost-benefit of switching to this technology, regarding both time and money, should be evaluated by an ethics committee within each hospital before its implementation. Additionally, animal experimentation for the analysis of material-tissue interactions, as well as for the surgeons training, must be further discussed. However, the promising applications of this new technology make it worth investing on, since its remote and precise motion control of surgical tools could inevitably lead to a new generation of minimal invasive surgical tools, creating a positive impact on society through the improvement of recovery time for the patients after surgery, as well as by facilitating the job to trained surgeons and increasing successful rate of procedures.

References

[1] M. Feng, Y. Fu, B. Pan, and C. Liu, "Development of a medical robot system for minimally invasive surgery," *The International Journal of Medical Robotics and Computer Assisted Surgery*, vol. 8, no. 1, pp. 85–96. [Online]. Available: https://onlinelibrary.wiley.com/doi/abs/10.1002/rcs.440

[2] M. Tonutti, D. S. Elson, G.-Z. Yang, A. W. Darzi, and M. H. Sodergren, "The role of technology in minimally invasive surgery: state of the art, recent developments and future directions," *Postgraduate Medical Journal*, vol. 93, no. 1097, pp. 159–167, 2017. [Online]. Available: https://pmj.bmj.com/content/93/1097/159

[3] G. Dogangil, B. L. Davies, and F. R. y Baena, "A review of medical robotics for minimally invasive soft tissue surgery," *Proceedings of the Institution of Mechanical Engineers, Part H: Journal of Engineering in Medicine*, vol. 224, no. 5, pp. 653–679, 2010, pMID: 20718269. [Online]. Available: https://doi.org/10.1243/09544119JEIM591

[4] B. Davies, "A review of robotics in surgery," *Proceedings of the Institution of Mechanical Engineers, Part H: Journal of Engineering in Medicine*, vol. 214, no. 1, pp. 129–140, 2000, pMID: 10718057. [Online]. Available: https://doi.org/10.1243/0954411001535309

[5] A. R. Lanfranco, A. E. Castellanos, J. P. Desai, and W. C. Meyers, "Robotic surgery: a current perspective," *Annals of surgery*, vol. 239, no. 1, p. 14, 2004.

[6] R. H. Taylor, A. Menciassi, G. Fichtinger, P. Fiorini, and P. Dario, *Medical Robotics and Computer-Integrated Surgery*. Cham: Springer International Publishing, 2016, pp. 1657–1684. [Online]. Available: https://doi.org/10.1007/978-3-319-32552-1_63

[7] M. Cianchetti and A. Menciassi, "Soft robots in surgery," in *Soft Robotics: Trends, Applications and Challenges*, C. Laschi, J. Rossiter, F. Iida, M. Cianchetti, and L. Margheri, Eds. Cham: Springer International Publishing, 2017, pp. 75–85.

[8] D. Rus and M. T. Tolley, "Design, fabrication and control of soft robots," *Nature*, vol. 521, pp. 467 EP –, May 2015. [Online]. Available: http://dx.doi.org/10.1038/nature14543

[9] W. Wang, Z. Yao, J. C. Chen, and J. Fang, "Composite elastic magnet films with hard magnetic feature," *Journal of Micromechanics and Microengineering*, vol. 14, no. 10, pp. 1321–1327, 2004.

[10] H. Li, T. J. Flynn, J. C. Nation, J. Kershaw, L. S. Stephens, and C. A. Trinkle, "Photopatternable ndfeb polymer micromagnets for microfluidics and microrobotics applications," *Journal of Micromechanics and Microengineering*, vol. 23, no. 6, 2013.

[11] J. Kim, S. E. Chung, S.-E. Choi, H. Lee, J. Kim, and S. Kwon, "Programming magnetic anisotropy in polymeric?microactuators," *Nature Materials*, vol. 10, pp. 747 EP –, Aug 2011. [Online]. Available: http://dx.doi.org/10.1038/nmat3090

[12] V. Q. Nguyen, A. S. Ahmed, and R. V. Ramanujan, "Morphing soft magnetic composites," *Advanced Materials*, vol. 24, no. 30, pp. 4041–4054. [Online]. Available: https://onlinelibrary.wiley.com/doi/abs/10.1002/adma.201104994

[13] T. Budde and H. H. Gatzen, "Thin film smco magnets for use in electromagnetic microactuators," *Journal of applied physics.*, vol. 99, no. 8 3, p. 8N304, 2006.

[14] K. Zhang, A. J. Krafft, R. Umathum, F. Maier, W. Semmler, and M. Bock, "Real-time mr navigation and localization of an intravascular catheter with ferromagnetic components," *Magnetic Resonance Materials in Physics, Biology and Medicine : Official Journal of the European Society for Magnetic Resonance in Medicine and Biology*, vol. 23, no. 3, pp. 153–163, 2010.

[15] C. Chautems and B. J. Nelson, "The tethered magnet: Force and 5-dof pose control for cardiac ablation," pp. 4837–4842, May 2017.

[16] Q. Ramadan, V. D. Samper, D. P. Puiu, and C. Yu, "Fabrication of three-dimensional magnetic microdevices with embedded microcoils for magnetic potential concentration," *Journal of Microelectromechanical Systems*, vol. 15, no. 3, pp. 624–638, 2006.

[17] B. L. Gray, "A review of magnetic composite polymers applied to microfluidic devices," *Journal of the Electrochemical Society*, vol. 161, no. 2, pp. B3173–B3183, January 01 2014.

[18] S. Yim and M. Sitti, "Design and rolling locomotion of a magnetically actuated soft capsule endoscope," *IEEE Transactions on Robotics*, vol. 28, no. 1, pp. 183–194, Feb 2012.

[19] S. Miyashita, S. Guitron, K. Yoshida, S. Li, D. D. Damian, and D. Rus, "Ingestible, controllable, and degradable origami robot for patching stomach wounds," pp. 909–916, May 2016.

[20] A. D. Losey, P. Lillaney, A. J. Martin, D. L. Cooke, M. W. Wilson, B. R. H. Thorne, R. S. Sincic, R. L. Arenson, M. Saeed, and S. W. Hetts, "Magnetically assisted remote-controlled endovascular catheter for interventional mr imaging: In vitro navigation at 1.5 t versus x-ray fluoroscopy," *Radiology*, vol. 271, no. 3, pp. 862–869, 2014, pMID: 24533872. [Online]. Available: https://doi.org/10.1148/radiol.14132041

[21] F. Settecase, M. S. Sussman, M. W. Wilson, S. Hetts, R. L. Arenson, V. Malba, A. F. Bernhardt, W. Kucharczyk, and T. P. L. Roberts, "Magnetically-assisted remote control (marc) steering of endovascular catheters for interventional mri: A model for deflection and design implications," *Medical physics*, vol. 34, no. 8, pp. 3135–3142, 2007.

[22] T. P. L. Roberts, W. V. Hassenzahl, S. W. Hetts, and R. L. Arenson, "Remote control of catheter tip deflection: An opportunity for interventional mri," *Magnetic Resonance in Medicine*, vol. 48, no. 6, pp. 1091–1095, 2002.

[23] M. S. Choi, Y.-S. Oh, S. W. Jang, J. H. Kim, W. S. Shin, H.-J. Youn, W. S. Jung, M. Y. Lee, and K. B. Seong, "Comparison of magnetic navigation system and conventional method in catheter ablation of atrial fibrillation: Is magnetic navigation system is more effective and safer than conventional method?" *Korean Circ J*, vol. 41, no. 5, pp. 248–252, May 2011. [Online]. Available: http://synapse.koreamed.org/DOIx.php?id=10.4070%2Fkcj.2011.41.5.248

[24] F. N. Pirmoradi, J. K. Jackson, H. M. Burt, and M. Chiao, "On-demand controlled release of docetaxel from a battery-less mems drug delivery device," *Lab Chip*, vol. 11, pp. 2744–2752, 2011. [Online]. Available: "http://dx.doi.org/10.1039/C1LC20134D"

[25] F. N. Pirmoradi, J. K. Jackson, H. M. Burt, and M. Chiao, "A magnetically controlled mems device for drug delivery: design, fabrication, and testing," *Lab on a Chip*, vol. 11, no. 18, pp. 3072–3080, 2011.

[26] P. Garstecki, P. Tierno, D. B. Weibel, F. SagueÌs, and G. M. Whitesides, "Propulsion of flexible polymer structures in a rotating magnetic field," *Journal of Physics: Condensed Matter*, vol. 21, no. 20, 2009.

[27] W. Hu, G. Z. Lum, M. Mastrangeli, and M. Sitti, "Small-scale soft-bodied robot with multimodal locomotion," *Nature*, vol. 554, pp. 81 EP –, Jan 2018. [Online]. Available: http://dx.doi.org/10.1038/nature25443

[28] E. Diller, J. Zhuang, G. Z. Lum, M. R. Edwards, and M. Sitti, "Continuously distributed magnetization profile for millimeter-scale elastomeric undulatory swimming," *Applied Physics Letters*, vol. 104, no. 17, p. 174101, 2014.

[29] B. D. Cullity and C. D. Graham, *Introduction to magnetic materials.* Hoboken, N.J.: IEEE/Wiley, 2009. [Online]. Available: http://site.ebrary.com/id/10303874

[30] W. D. J. Callister, *Materials science and engineering : an introduction.* New York: John Wiley & Sons, 2007. [Online]. Available: http://catdir.loc.gov/catdir/enhancements/fy0625/2005054228-t.html

[31] D. J. Griffiths, *Introduction to electrodynamics.* Harlow: Pearson, 2016.

[32] G. Filipcsei, I. Csetneki, A. Szilagyi, and M. Zrinyi, "Magnetic field-responsive smart polymer composites," *Advances In Polymer Science*, vol. 206, pp. 137–190, 2007.

[33] J. TheÌvenot, H. Oliveira, O. Sandre, and S. Lecommandoux, "Magnetic responsive polymer composite materials." *Chemical Society Reviews*, vol. 42, no. 17, pp. 7099–116, 2013.

[34] C. Heunis, J. Sikorski, and S. Misra, "Flexible instruments for endovascular interventions: Improved magnetic steering, actuation, and image-guided surgical instruments," *IEEE Robotics Automation Magazine*, pp. 1–1, 2018.

[35] I. D. Johnston, D. K. McCluskey, and M. C K L Tan and, "Mechanical characterization of bulk sylgard 184 for microfluidics and microengineering," *Journal of Micromechanics and Microengineering*, vol. 24, no. 3, p. 035017, 2014. [Online]. Available: http://stacks.iop.org/0960-1317/24/i=3/a=035017

[36] M. Pallapa and J. T. W. Yeow, "A review of the hybrid techniques for the fabrication of hard magnetic microactuators based on bonded magnetic powders," *Smart Materials and Structures*, vol. 24, no. 2, 2015.

[37] J. Sikorski, I. Dawson, A. Denasi, E. E. G. Hekman, and S. Misra, "Introducing bigmag x2014; a novel system for 3d magnetic actuation of flexible surgical manipulators," pp. 3594–3599, May 2017.

[38] A. Ghanbari, A. Rostami, S. M. R. S. Noorani, and M. M. S. Fakhrabadi, "Modeling and simulation of inchworm mode locomotion," pp. 617–624, 2008.

[39] B. A. Trimmer, "Animal models for non-pneumatic soft robots," in *Soft Robotics: Trends, Applications and Challenges*, C. Laschi, J. Rossiter, F. Iida, M. Cianchetti, and L. Margheri, Eds. Cham: Springer International Publishing, 2017, pp. 47–55.

[40] K. Kotay and D. Rus, "The inchworm robot: A multi-functional system," *Autonomous Robots*, vol. 8, no. 1, pp. 53–69, 2000.

[41] S. Seok, C. D. Onal, K. Cho, R. J. Wood, D. Rus, and S. Kim, "Meshworm: A peristaltic soft robot with antagonistic nickel titanium coil actuators," *IEEE/ASME Transactions on Mechatronics*, vol. 18, no. 5, pp. 1485–1497, Oct 2013.

[42] H. Lin, G. Leisk, and B. Trimmer, "Soft robots in space: a perspective for soft robotics," *Acta Futura*, vol. 6, pp. 69–79, 2013.

[43] L. Phee, D. Accoto, A. Menciassi, C. Stefanini, M. C. Carrozza, and P. Dario, "Analysis and development of locomotion devices for the gastrointestinal tract," *IEEE Transactions on Biomedical Engineering*, vol. 49, no. 6, pp. 613–616, June 2002.

[44] B. Kim, H. Y. Lim, J. H. Park, and J.-O. Park, "Inchworm-like colonoscopic robot with hollow body and steering device," *JSME International Journal Series C Mechanical Systems, Machine Elements and Manufacturing*, vol. 49, no. 1, pp. 205–212, 2006.

[45] E. H. Hasnaa and B. Mohammed, "Planning tripod gait of an hexapod robot," in *2017 14th International Multi-Conference on Systems, Signals Devices (SSD)*, March 2017, pp. 163–168.

[46] B. You, Y. Shi, Y. Liu, and N. Li, "Analysis of tripod gait and research on controlling technology of hexapod robot," in *Ifost*, vol. 1, June 2013, pp. 725–728.

[47] P. Ramdya, R. Thandiackal, R. Cherney, T. Asselborn, R. Benton, A. J. Ijspeert, and D. Floreano, "Climbing favours the tripod gait over alternative faster insect gaits," *Nature Communications*, vol. 8, pp. 14 494 EP –, Feb 2017, article. [Online]. Available: http://dx.doi.org/10.1038/ncomms14494

[48] R. F. Shepherd, F. Ilievski, W. Choi, S. A. Morin, A. A. Stokes, A. D. Mazzeo, X. Chen, M. Wang, and G. M. Whitesides, "Multigait soft robot," *Proceedings of the National Academy of Sciences*, vol. 108, no. 51, pp. 20 400–20 403, 2011. [Online]. Available: http://www.pnas.org/content/108/51/20400

[49] D. Drotman, S. Jadhav, M. Karimi, P. deZonia, and M. T. Tolley, "3d printed soft actuators for a legged robot capable of navigating unstructured terrain," in *2017 IEEE International Conference on Robotics and Automation (ICRA)*, May 2017, pp. 5532–5538.

[50] F. F, P. MW, and van Ijzendoorn LJ, "Micro-fluidic actuation using magnetic artificial cilia." *Lab on a chip*, vol. 9, no. 23, pp. 3413–21, 2009.

[51] S. Hanasoge, P. J. Hesketh, and A. Alexeev, "Microfluidic pumping using artificial magnetic cilia," *Microsystems & Nanoengineering*, vol. 4, no. 1, p. 11, 2018. [Online]. Available: https://doi.org/10.1038/s41378-018-0010-9

[52] S. N. Khaderi, J. M. den Toonder, and P. R. Onck, "Chapter one - magnetic artificial cilia for microfluidic propulsion," ser. Advances in Applied Mechanics, S. P. Bordas and D. S. Balint, Eds. Elsevier, 2015, vol. 48, pp. 1 – 78. [Online]. Available: http://www.sciencedirect.com/science/article/pii/S0065215615000022

[53] M. E. Miller, M. Siegler, and P. Angelos, "Ethical issues in surgical innovation," *World Journal of Surgery*, vol. 38, no. 7, pp. 1638–1643, Jul 2014. [Online]. Available: https://doi.org/10.1007/s00268-014-2568-1

[54] J. A. Larson, M. H. Johnson, and S. B. Bhayani, "Application of surgical safety standards to robotic surgery: Five principles of ethics for nonmaleficence," *Journal of the American College of Surgeons*, vol. 218, no. 2, pp. 290 – 293, 2014. [Online]. Available: http://www.sciencedirect.com/science/article/pii/S1072751513011939

[55] B. D. Ratner, "Biomaterials science : an introduction to materials in medicine," [Place of publication not identified], 2013. [Online]. Available: http://public.eblib.com/choice/publicfullrecord.aspx?p=1074425

[56] H. W. F. Sung and C. Rudowicz, "Physics behind the magnetic hysteresis loopâa survey of misconceptions in magnetism literature," *Journal of Magnetism and Magnetic Materials*, vol. 260, no. 1, pp. 250–260, 2003.

[57] T. Speliotis, D. Niarchos, P. Falaras, D. Tsoukleris, and J. Pepin, "Nd-fe-b thick films prepared by screen printing," *IEEE Transactions on Magnetics Mag*, vol. 41, no. 10, pp. 3901–3903, 2005.

[58] Y. Kim, H. Yuk, R. Zhao, S. A. Chester, and X. Zhao, "Printing ferromagnetic domains for untethered fast-transforming soft materials," *Nature*, 2018.

5 Appendices

A Magnetic Theory

Magnetism is the phenomenon by which materials assert an attractive or repulsive force or influence on other materials. All substances are influenced to one degree or another by the presence of a magnetic field. The macroscopic magnetic properties of materials are a consequence of magnetic moments associated with individual electrons. (The information and figures contained in this appendix were obtained from [29][30][31][56]).

Origins of Magnetic Moments

Each electron in an atom has magnetic moments that originate from two sources: orbital and spin motion. The orbital motion corresponds to the movement of the electron around the nucleus; being a moving charge, the electron may be considered to be a small current loop, generating a very small magnetic field, with a corresponding magnetic moment along its axis of rotation.

Also, each electron may be thought of as spinning around an axis; this originates other magnetic moment along the spin axis. Spin magnetic moments may be only in an "up" or "down" direction. Thus each electron in an atom can be seen as a small magnet having permanent orbital and spin magnetic moments (see Figure 20).

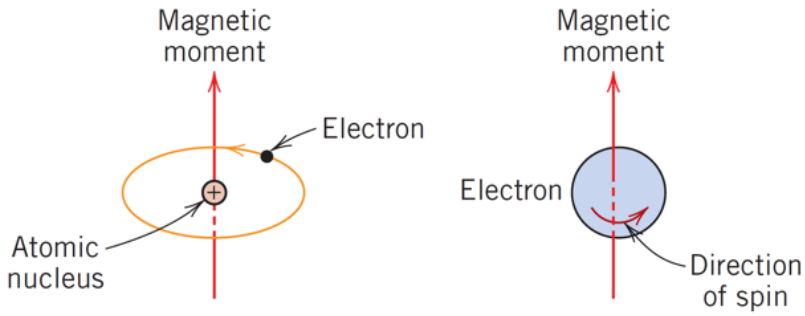

Figure 20: Origin of the two magnetic moments in an atom: orbital movement (left) and electron spin (right).

In each individual atom, orbital and spin moments of some electron pairs can cancel each other; for example, the spin moment of an electron with spin up will cancel that of one with spin down. As a result, the net magnetic moment for an atom is the sum of the magnetic moments of each of the constituent electrons, including both orbital and spin contributions, and taking into account moment cancellation. This means that, for an atom having completely filled electron shells or subshells, when all electrons are considered, there is total cancellation of both orbital and spin moments. Depending on the response of atomic magnetic dipoles, then, the magnetic behavior of materials can be classify in diamagnetism, paramagnetism, ferromagnetism, antiferromagnetism and ferrimagnetism.

Diamagnetism. A diamagnetic substance is composed of atoms which have no net magnetic moment. This type of magnetism is induced by a change in the orbital motion of electrons due to an external magnetic field. The theory considers that the applied field reduces the effective current of the orbit, generating a magnetic moment in the opposite direction of the field. The magnitude of the induced magnetic moment is extremely small and can only be observed when other types of magnetism are absent.

Paramagnetism. Paramagnetic materials consist of atoms, or molecules, which have the same net magnetic moment due to incomplete cancellation of electron spin/orbital components. In absence of an external field, these magnetic moments are randomly oriented and cancel one another, resulting in no net macroscopic

magnetization. However, when a field is applied, the atomic dipoles rotate and align in the direction of the external field; this results in the material acquiring a net magnetic moment. Thermal agitation of the atoms opposes the alignment and keeps the atomic dipoles pointing at random, which decreases the macroscopic magnetic moment.

Ferromagnetism. Ferromagnetic materials possess a permanent magnetic moment in the absence of an external field, and have very large and permanent magnetizations. The permanent magnetic moments results from atomic magnetic moments mainly due to uncancelled electron spins, and a small contribution from orbital moment as well. The difference with paramagnets is that, in this case, dipoles of neighboring atoms interact with each other and tend to align in the same direction. This creates microscopic volume regions with a net magnetic moment in the material called domains. When an external field is applied, all the domains align in the same direction of the field. Once the field is remove, although some domains may change their orientation due to thermal agitation, in general, the alignment is preserved, making possible for the material to conserve a large magnetic moment.

Antiferromagnetism and Ferrimagnetism. In antiferromagnetic substances, the dipole moment between adjacent atoms or ions couples antiparallel to each other. As a result, the substance has no net magnetic moment, but can acquire one when a strong field is applied to it. Ferrimagnetic materials have a permanent magnetic moment, similar to ferromagnets. However, the origin of this moment is what differentiates both groups. In ferromagnetism, the magnetization originates when antiparallel spin-coupling interactions, just like antiferromagnets, do not cancel each other completely.

Magnetization and Hysteresis curve

As introduced in the previous section, ferro- and ferrimagnetic materials are constituted by microscopic regions called domains. Each domain is magnetized spontaneously up to its saturation. However, a single material is composed of a large number of domains, each with a moment pointing in a random direction, resulting in no net macroscopic magnetization. The magnetization process consists in applying an external magnetic field in order to align all the domains (Figure 21). When this occurs, the specimen achieves its maximum magnetization, the saturation magnetization M_s.

The behavior of the magnetic moment with respect to the external applied field results in a plot similar to the one shown in Figure 22. In ferromagnetic materials, a non-linear relation can be observed in this type of plot. An unmagnetized specimen starts at the origin, as the external field H increases, the induced magnetic moment M begins to increase slowly, then more rapidly, and finally levels when it reaches saturation. When the field H decreases, the maintained alignment of the domains retains certain degree of magnetization. In the point at which H_{ci}=0, the magnetic moment retained is called remanence, or remanent magnetization M_r. The extension of this plot to negative values, and then its returning to positives values of the external field H, completes the M-H curve, with a clear hysteresis phenomenon. Another important point is where the field reduces the magnetic moment to zero, this point is identify as the intrinsic coercivity, H_{ci}.

Ferromagnetic materials can be classify as soft or hard, based on their hysteresis curve (Figure 23). Soft magnetic materials are characterized by low field to reach saturation and low H_{ci}, meaning that can be easily magnetized and demagnetized. On the other hand, hard magnetic material requires higher fields to reach saturation, and have higher magnetic remanence and H_{ci}. For the reason, these materials are usually known as permanent magnets. In paramagnetic materials, the achieved magnetic moment is much lower, it keeps a linear relation with the external field H, and there is no hysteresis observed. However, a subgroup called superparamagnetics, is able to have a non-linear and high magnetization, just as ferromagnets, with no hysteresis (Figure 24).

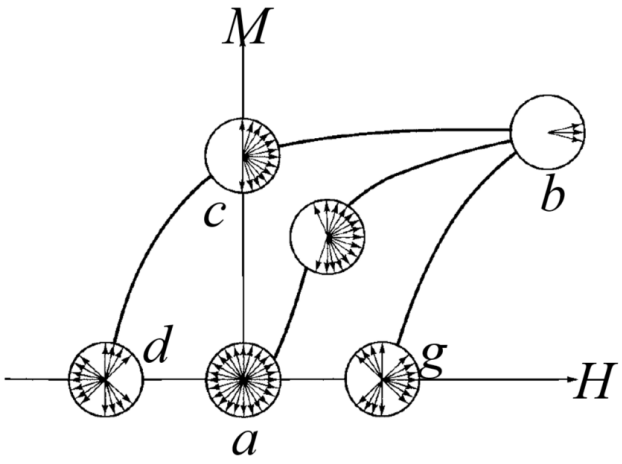

Figure 21: Behaviour of magnetic domains at the principal points of a magnetization process. Points indicated correspond to the ones in Figure 22.

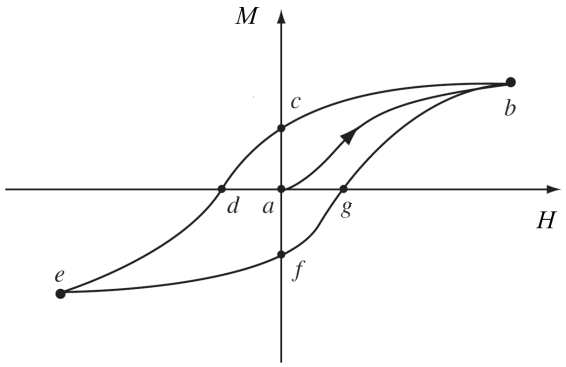

Figure 22: M-H curve of a ferromagnetic material with the main magnetic properties obtained from the plot: magnetic saturation, M_s (point b, e); magnetic remanence, M_r (point c, f); and intrinsic coercivity, H_{ci} (point d, g). Point a correspond to an initial unmagnetized state.

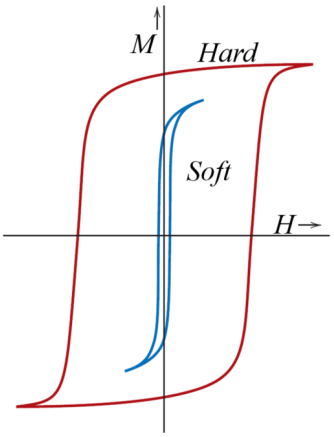

Figure 23: Behaviour of soft and hard magnetic materials. It can be observe that hard magnetic materials have higher values for remanence and coercivity. The lower values in soft magnetic materials allows its easy magnetization and demagnetization.

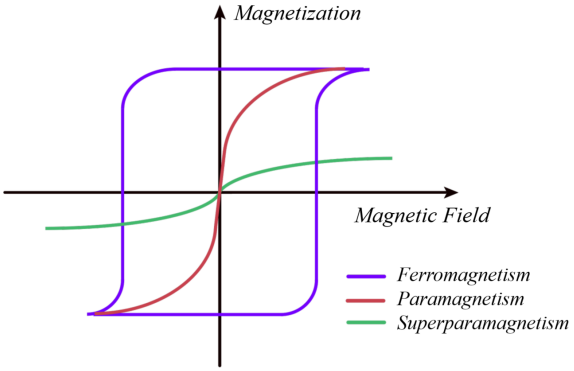

Figure 24: M-H curve for ferromagnetic, paramagnetic and superparamagnetic materials. Only ferromagnetic materials have an hysteresis behavior.

B Calculations (permanent magnets)

Relevant information about the permanent magnet used to conduct the preliminary tests can be found in the following table.

Article ID	S-60-05-N
Material	NdFeB
Shape	Disc
Diameter	60 mm
Height	5 mm
Direction of magnetization	Axial (parallel to height)
Magnetization	N42
B_r	1.29 – 1.32 T

The magnetic flux density B given in axial direction by a cylinder magnet is given by:

$$B = \frac{B_r}{2}\left(\frac{T+z}{\sqrt{R^2+(T+z)^2}} - \frac{z}{\sqrt{R^2+z^2}}\right), \tag{3}$$

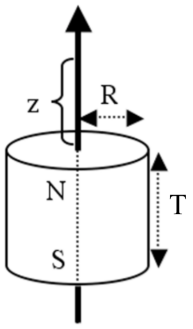

Figure 25: Cylindrical magnet model.

where $\mathbf{B_r}$ is remanence field in the magnet; $\mathbf{z}$ is the distance from a pole face on the symmetrical axis; $\mathbf{T}$ is the thickness (or height) of the cylinder; and $\mathbf{R}$ is the radius of the cylinder (see Figure 25).

When the magnetic fields of two magnets interact with each other, the resultant field is generated following the principle of superposition; this occurs in the different holders created to do the preliminary tests. The field between two identical cylindrical magnets is given by:

$$B = \frac{B_r}{2}\left(\frac{x_1+T}{\sqrt{R^2+(x_1+T)^2}} - \frac{x_1}{\sqrt{R^2+x_1^2}} + \frac{x_2+T}{\sqrt{R^2+(x_2+T)^2}} - \frac{x_2}{\sqrt{R^2+x_2^2}}\right), \tag{4}$$

with $\mathbf{x_1} = (\mathbf{d/2}) + \mathbf{x}$ and $\mathbf{x_2} = (\mathbf{d/2}) - \mathbf{x}$; $\mathbf{d}$ is the distance between the two magnets; and $\mathbf{x}$ is the distance from the middle point between the magnets to the point of interest (see Figure 26).

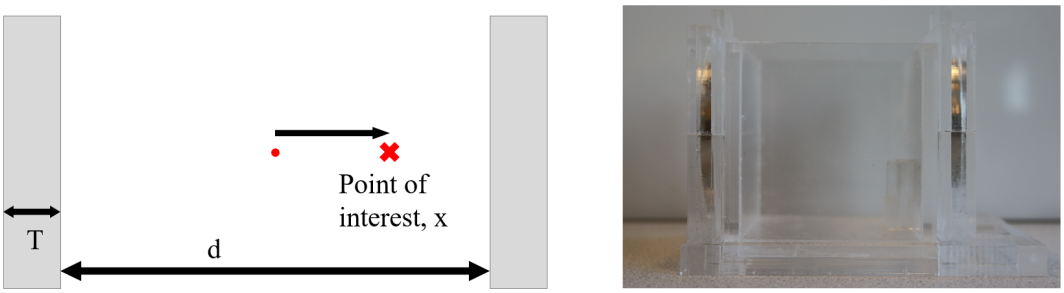

Figure 26: (Left) Model to apply Equation (4). (Right) Holder fabricated to do test.

According to Equation (4), the magnetic field in the axial line inside the holder goes from 50 mT in the regions nearest to the magnet, to 23 mT in the middle point.

The magnetic flux density of a dipole moment in any direction can be calculated as:

$$B(r) = \frac{\mu_0}{4\pi}\left(\frac{3\mathbf{r}(\mathbf{m}\cdot\mathbf{r})}{|r|^5} - \frac{\mathbf{m}}{|r|^3}\right) \tag{5}$$

where μ_0 is the permeability of free space ($4\pi \cdot 10^{-7} Hm^{-1}$; $\mathbf{r}$ is the position vector; $\mathbf{m}$ is the magnetic moment vector.

Equation (5) was used to calculate the direction of the field during the crawling motion in Figure 11. The permanent magnet was taken as a punctual dipole with a moment purely in its axial direction, and the point of interest was taken somewhere in the middle of the sample (see Figure 29). Using different frames of the movement it was possible to obtained the values of the angle at which the magnetic field acts on the sample (see Table 5).

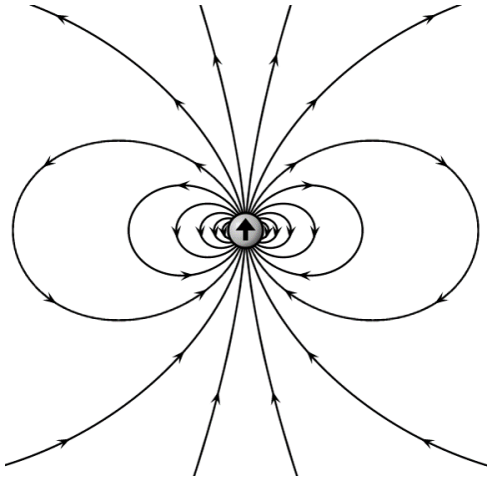

Figure 27: Magnetic field around a dipole represented by field lines.

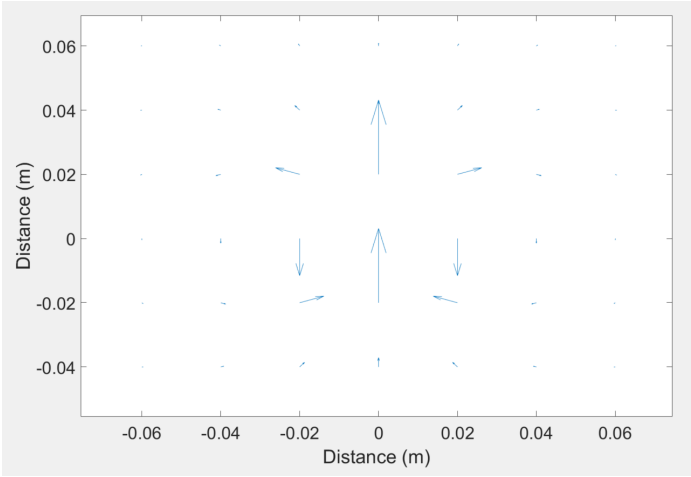

Figure 28: Representation of the intensity and direction of the magnetic field generated by a punctual dipole using Equation (5).

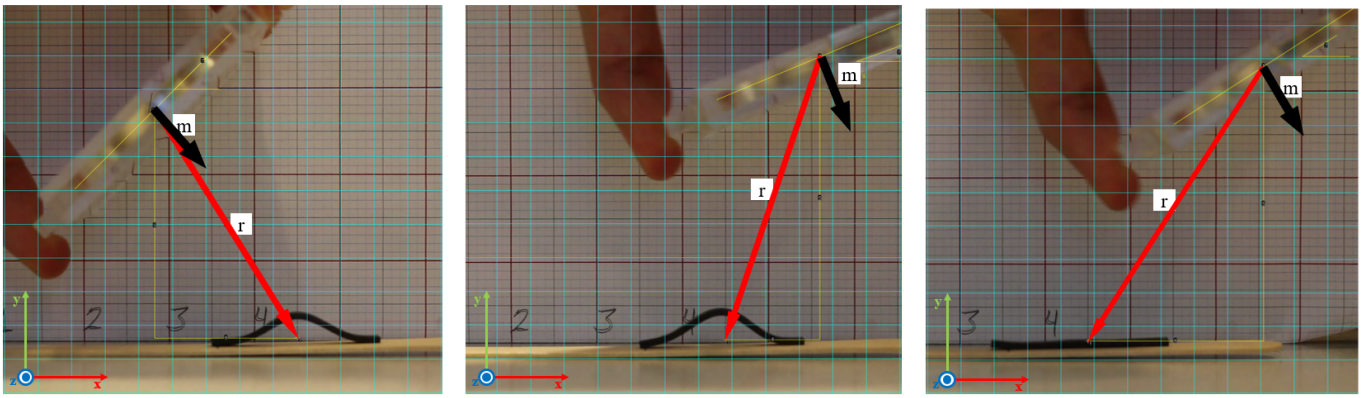

Figure 29: Defined *mathbfm* and *mathbfr* vectors in order to approximate the direction of the field at the point of interest.

Table 5: Angles obtained for a cycle of movement. The angles are with respect the positive x-axis.

Frame	Field angle (degrees)
scene31	119.4787447
scene36	116.3384482
scene56	102.5292481
scene91	50.14983246
scene96	10.84154935

C Fabrication Techniques

Common techniques employed for polymer fabrication that can also be used for the fabrication of MPC's are briefly described in the next table.

Fabrication Technique	Description	Limitations
Screen printing [36][57]	The method uses a mesh with the desired pattern on it. Ink is poured over the mesh and after a squeegee pass over it, the pattern is transferred to the substrate below. The earlier the mixture is wiped onto the substrate, the thinner it is.	Viscosity of the ink should be low. Mixture left on the substrate is not very uniform.
Moulding processing [9][36]	This method uses a master mold with the desired pattern fabricated by other techniques such as lithography, laser ablation, injection molding, etc. This master can be done in either rigid or soft material. The composite is then cast and cured in this mold.	Presence of air bubbles in the substrate-composite interface.
Squeegee-coating processing [9][36]	A rigid patterned substrate is used as mold. The uncured composite is poured into the mold, so it can flow into the cavities. The excess of material is removed by passing a flat edge across the substrate. Since the mold can be prepared by different methods, it is possible to have different depths of the cavities on the same mold.	Viscosity of the composite limits the minimum cavity feature size.
Spin casting [36]	In this technique a centrifugal force is used to distribute the composite over the mold. The desired geometry can be achieved by using patterned molds. Either thin or thick films can be fabricated depending on the parameters of spinning.	Difference in weight between the particles and polymer might lead to separation during centrifugation.
Inkjet printing [36][58]	Inkjet printing offers good control over lateral geometries and the thickness can be controlled with the number of printing passes. There is no need for demolding or extra chemical techniques, and sandwich layers and devices can be fabricated with appropriated steps.	Viscosity of the ink should be low.

D VSM Data Analysis

The measurements of the magnetic properties is performed in a Vibrating-Sample Magnetometer (VSM, Quantum Design Inc). Four magnetization steps are performed to complete one measurement: 1) from 0 to 3 T; 2) from 3 T to -3 T; 3) from -3 T to 3 T; from 3 T to 0. For the data acquisition, the change in the external magnetic to go from the initial to the final value of each step is programmed to be 200 mT, except in the ranges between 0.5 and -0.5 T, where this change is programmed to be 40 mT. This increase the number of data points acquired between these ranges, allowing to have more precise values in the intersections with the axes. The time required for one measurement is approximately 30 minutes. The data is exported to Matlab for further analysis; three processing steps are performed to obtain the corresponding M-H curve of the material.

1. Data selection. From the four above mentioned magnetization steps, the second and the third one correspond to the M-H curve. So for further processing, only this data is taken into account (see Figure 30).

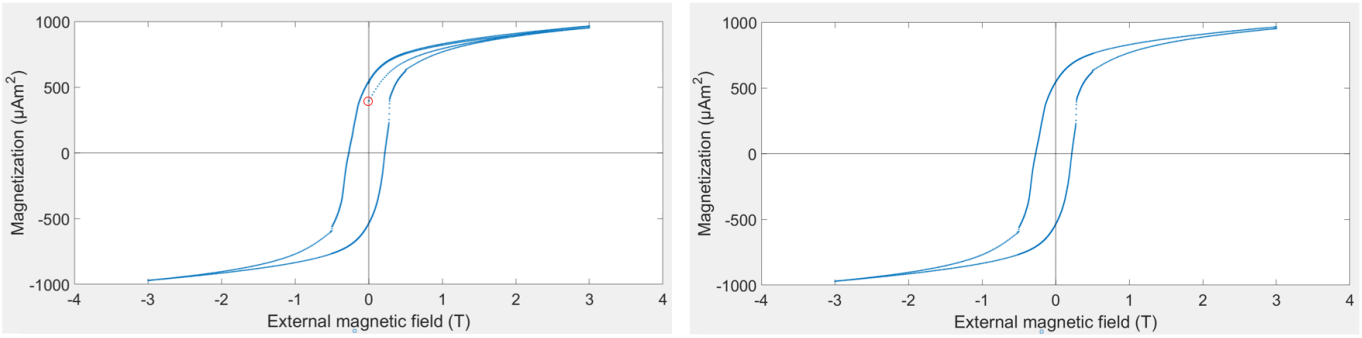

Figure 30: (Left) Plot of the complete data obtained from the VSM. Before the measurements on the device, the sample was magnetized under a uniform 1.5 T magnetic field. This causes that the curve does not start at 0 (demagnetized state), but with certain magnetization (circled in red). (Right) Plot corresponding to the magnetization steps from 3 T to -3 T, and vice versa.

2. Linearization of the both ends. Since the value obtained from the measurement in the y-axis is the magnetic moment, it should reach a saturation level. However, this is not observed in the plot, instead, saturation is observed at both ends by the switch to a linear relation between the external magnetic field and the magnetic moment of the sample. In order to obtain the correct plot, linearization (and further correction) of both ends needs to be done. According to the supplier of the magnetic microparticles, 95% of the material saturates with a field around 2 T, which can be corroborated by the data by the proximity to the linear behavior of the curve. After examining the data, saturation was defined at 2.5 T. Data from 2.5 to 3 T (and -2.5 to -3T) was used for linearization using the *Curve fitting* application in Matlab (Figure 31).

3. Correction. After obtaining the two functions that describes the linear behavior at both ends of the curve, a simple average is taken and subtracted from the entire data. Finally the new curve is plotted with a clear saturation level corresponding to the M-H curve (see Figure 32). Table 6 shows the values of the main magnetic properties obtained from the measurements.

Table 6: Magnetic properties obtained from the data before and after the correction.

Parameter	Before correction		After correction	
	Max.	Min.	Max.	Min.
H field (T)	3.0001	-3.0000	3.0001	3.0000
$M_s(\mu Am^2)$	964.9062	-970.5356	801.5597	-798.6873
$M_r(\mu Am^2)$	544.8610	-537.2206	549.1137	-532.9678
H_{ci} (mT)	-271.32	219.38	-278.67	221.18

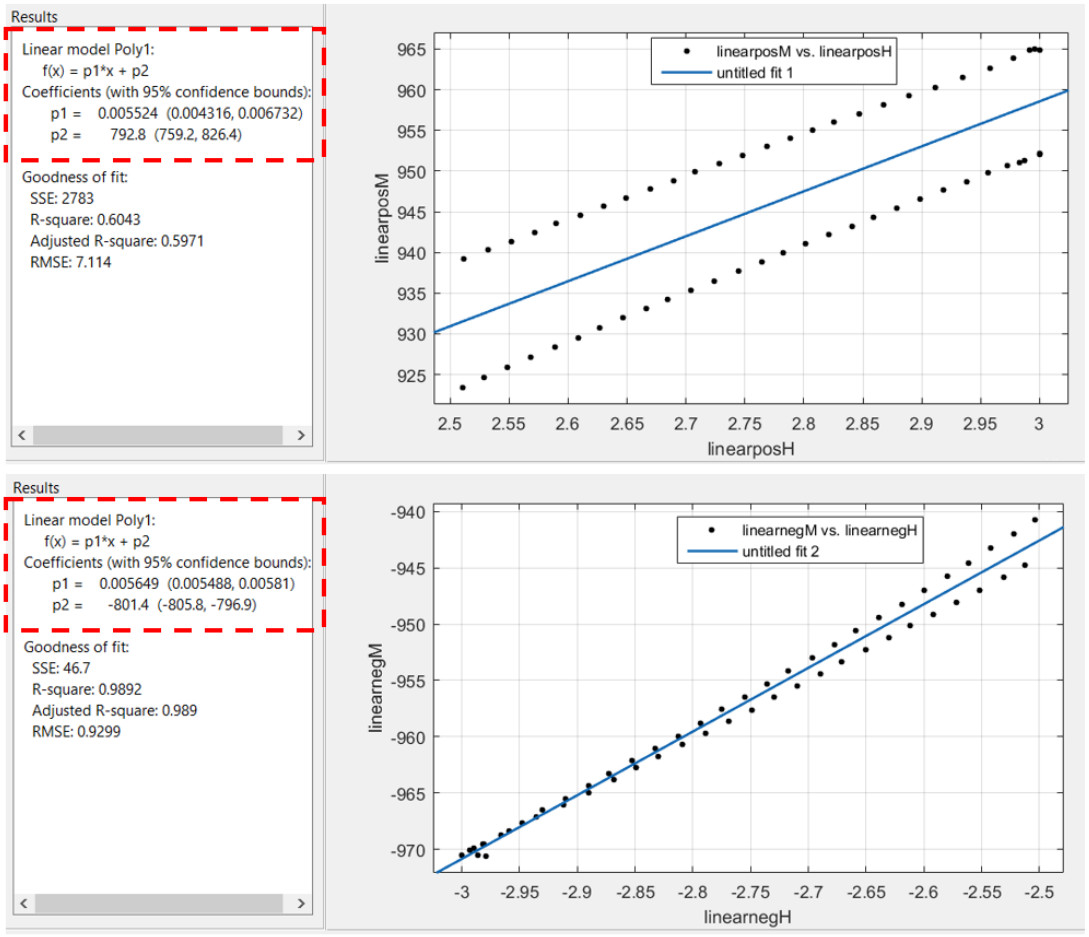

Figure 31: Data points from the positive (top) and negative end (bottom) with the corresponding linearization. Similar functions are obtained since the curve is theoretically symmetric.

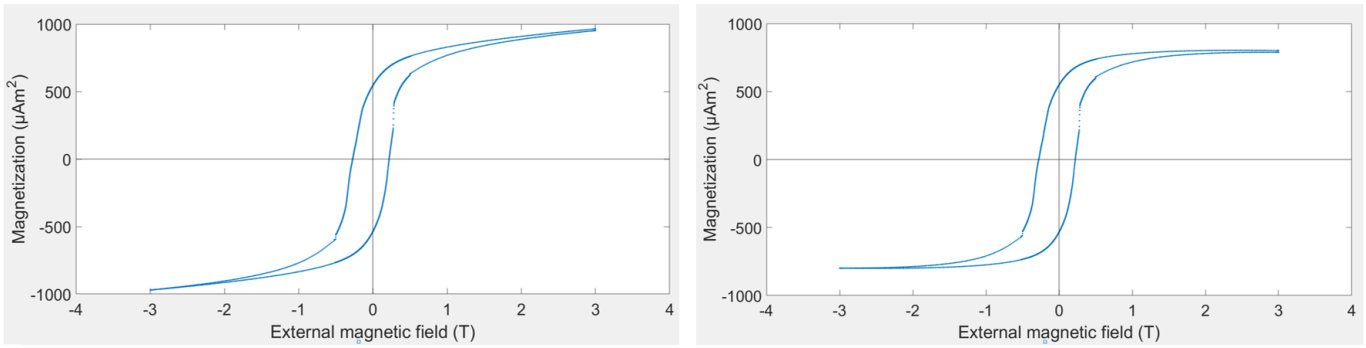

Figure 32: Original curve (left) and obtained corrected curve (right).

E Preliminary Tests

Platform | Circular base | Square base

Figure 33: Different holders used for the preliminary tests .

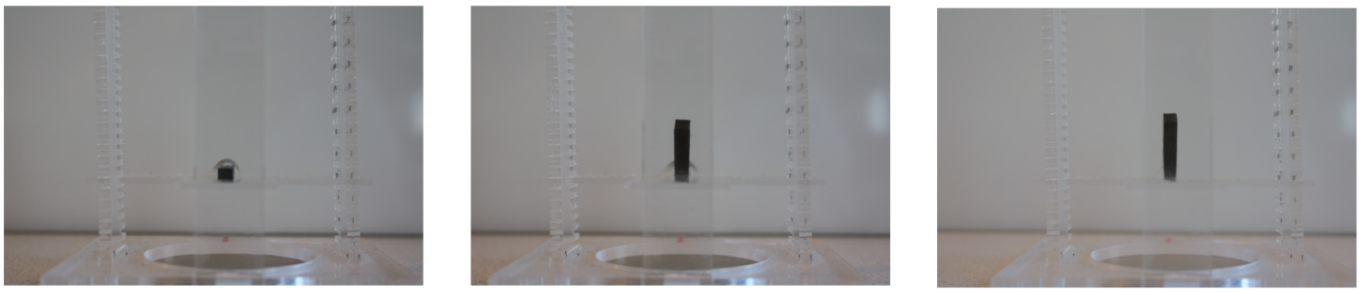

Ecoflex 2:1 (before magnetization) | Ecoflex 2:1 (after magnetization) | Ecoflex 1:1

Figure 34: Ecoflex samples before and after with axial magnetization. (Left) Sample at 2:1 weight ratio but non-magnetize. (Middle) Sample at 2:1 weight ratio with magnetic particles. (Right) Sample at 1:1 weight ratio with magnetic particles.

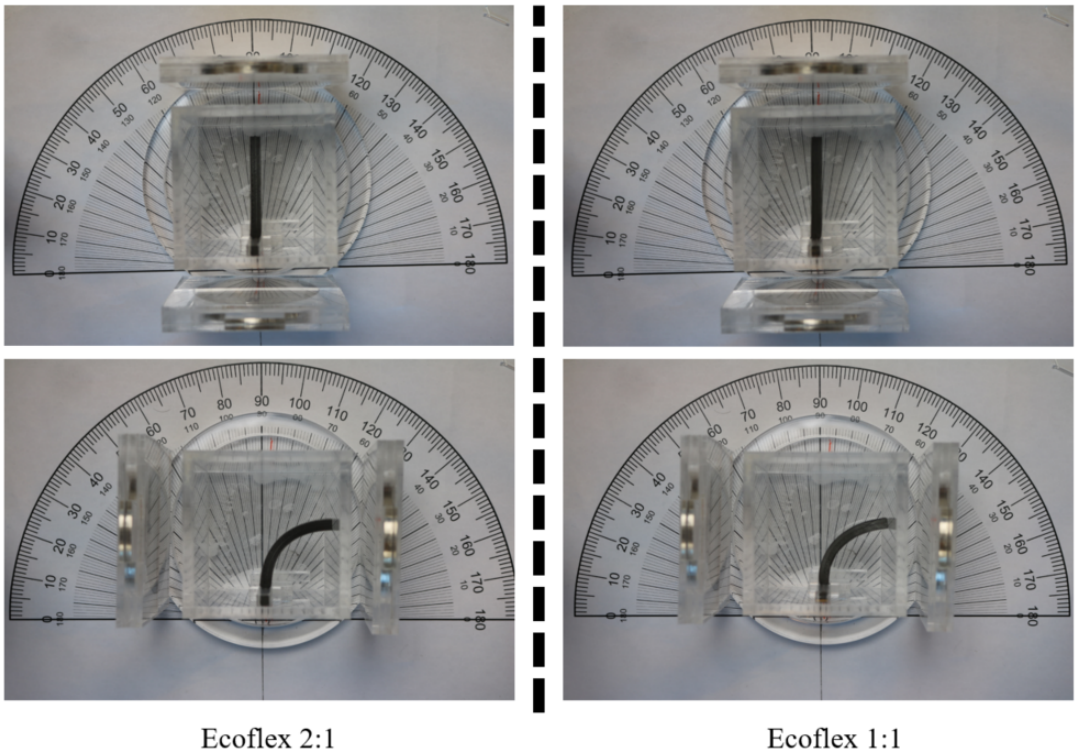

Ecoflex 2:1 | Ecoflex 1:1

Figure 35: Comparison between samples made of the same material but different particle concentration. (Left) Sample at 2:1 weight ratio with magnetic particles. (Right) Sample at 1:1 weight ratio with magnetic particles.

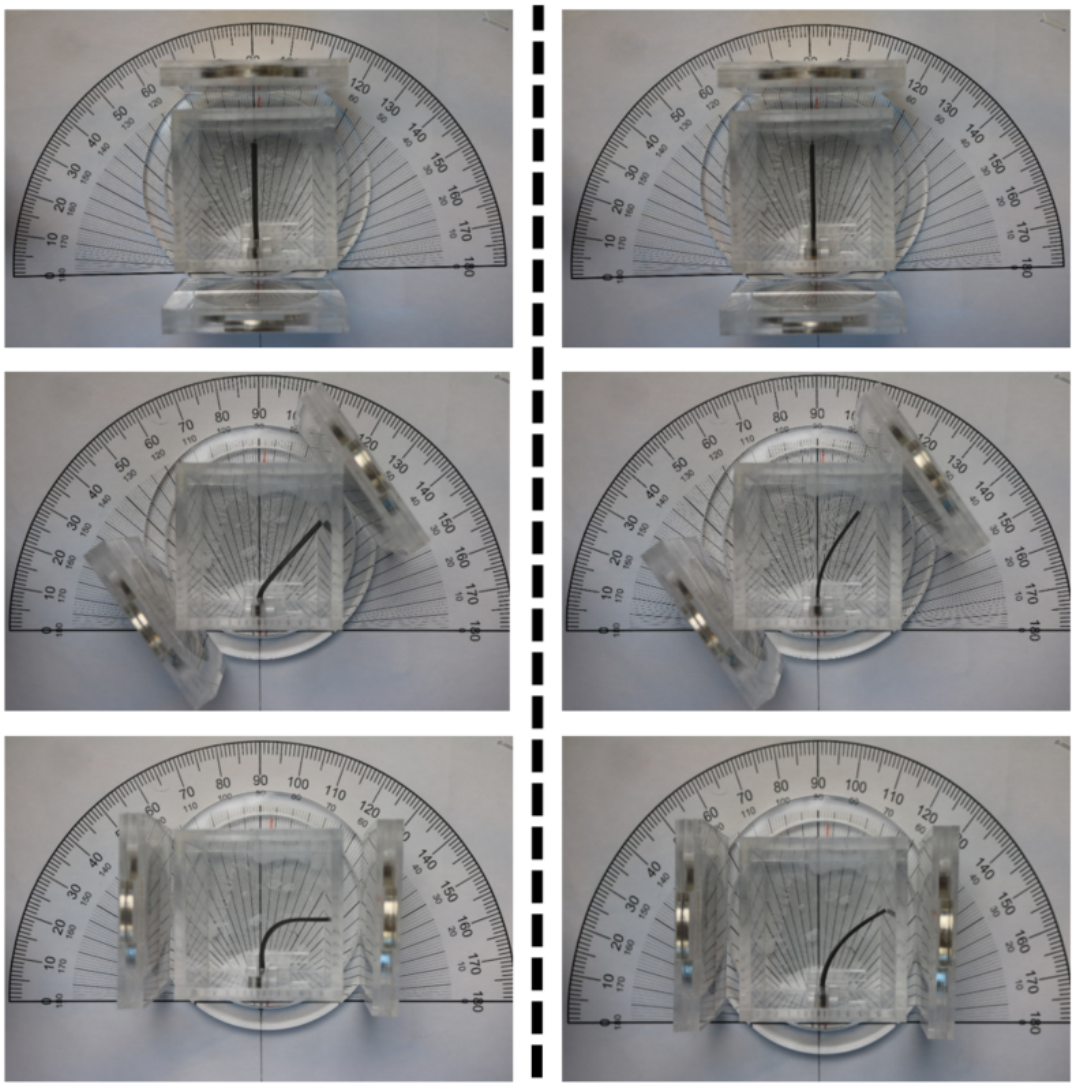

Figure 36: Comparison between samples made of different material but the same particle concentration. (Left) Ecoflex ample at 1:1 weight ratio with magnetic particles. (Right) PMC sample at 1:1 weight ratio with magnetic particles.

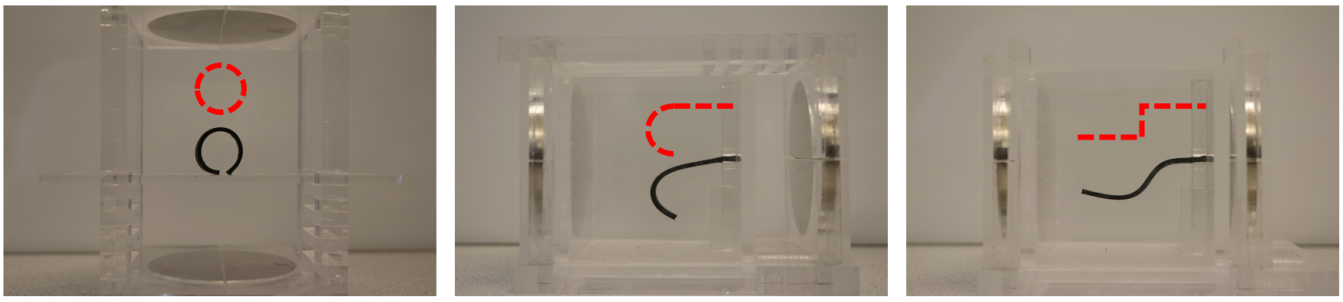

Figure 37: Ecoflex samples at 1:1 weight ratio with magnetic particles. Each sample deforms according to the magnetization profile (shown in red dashed curves) when exposed to an external field.

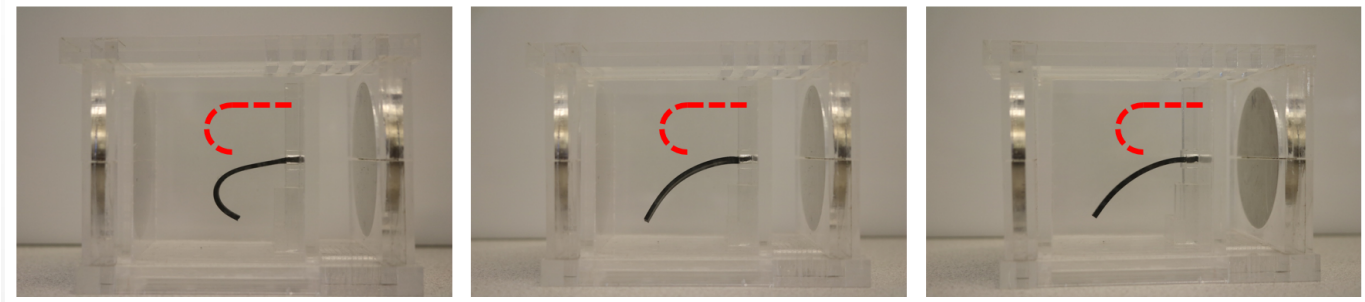

Figure 38: Same magnetization profile (indicated in dash lines) using different polymers: Ecoflex (left), PMC (middle), and PDMS (right). Ecoflex and PMC samples are made at 1:1 weight ratio; PDMS sample is made at 2:1 weight ratio. Ecoflex sample is the only one to deform accordingly to the magnetization profile thanks to its high compliance.

F Samples and magnetization profiles

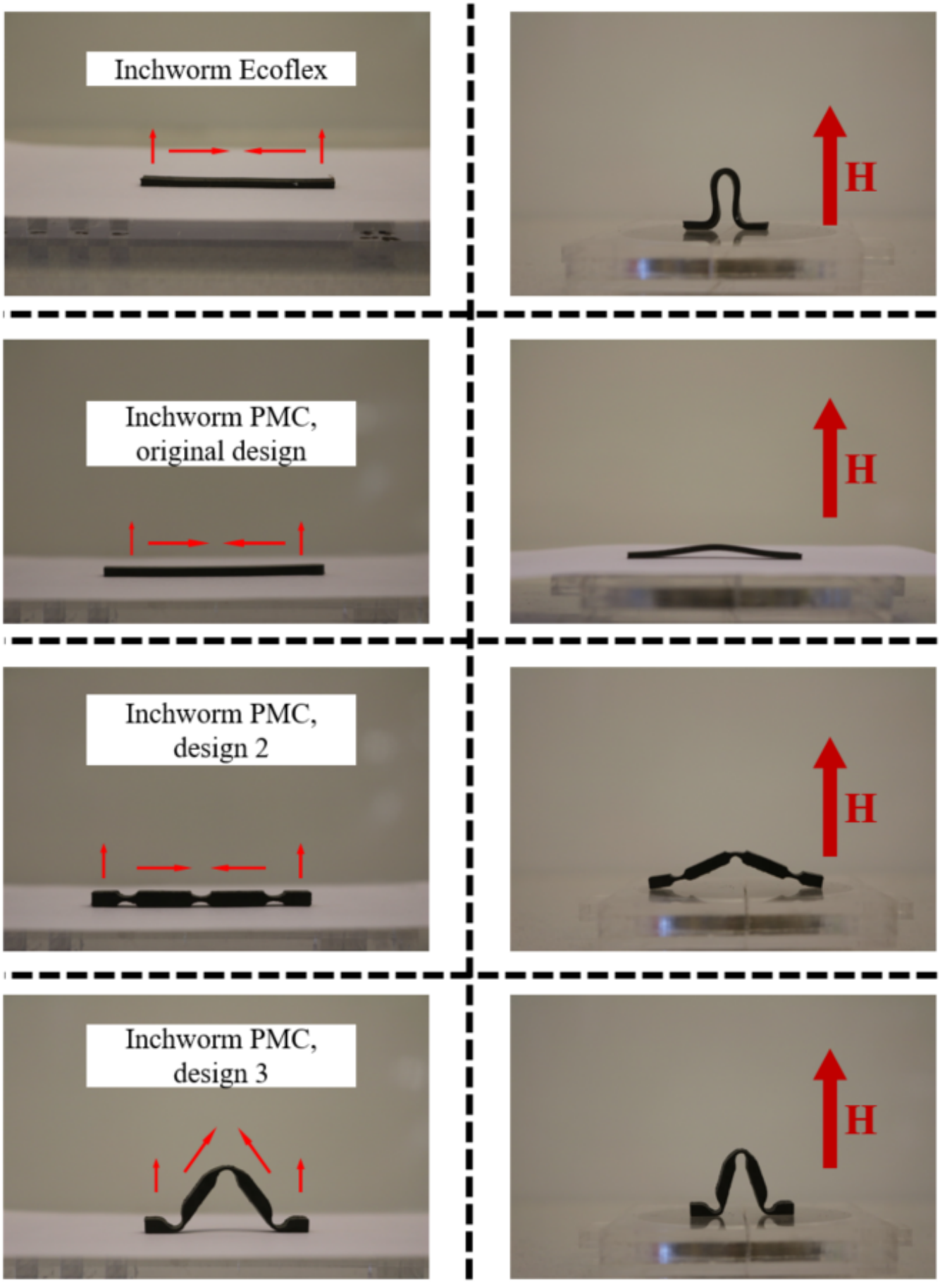

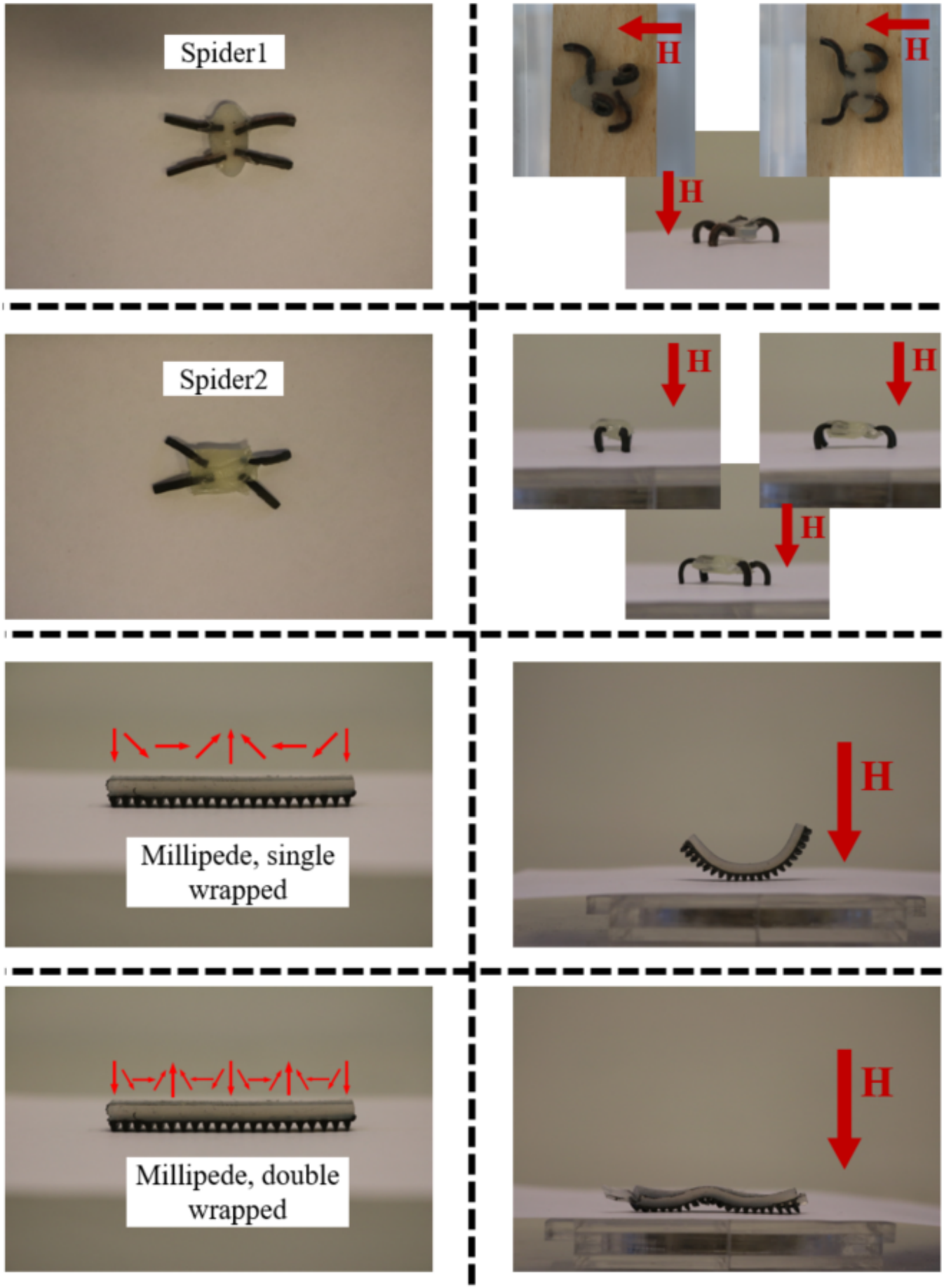
Spider1
H
H
H
Spider2
H
H
H
Millipede, single wrapped
H
Millipede, double wrapped
H